CHEMISTRY
A EUROPEAN JOURNAL

DOI: 10.1002/chem.200800799

Aromatic Hydroxylation in a Copper Bis(imine) Complex Mediated by a μ-η²:η² Peroxo Dicopper Core: A Mechanistic Scenario

Ole Sander,[a] Anja Henß,[b] Christian Näther,[a] Christian Würtele,[b] Max C. Holthausen,*[c] Siegfried Schindler,*[b] and Felix Tuczek*[a]

Dedicated to Professor Helmut Schwarz on the occasion of his 65th birthday

Abstract: Detailed mechanistic studies on the ligand hydroxylation reaction mediated by a copper bis(imine) complex are presented. Starting from a structural analysis of the Cu^{I} complex and the Cu^{II} product with a hydroxylated ligand, the optical absorption and vibrational spectra of starting material and product are analyzed. Kinetic analysis of the ligand hydroxylation reaction shows that O_2 binding is the rate-limiting step. The reaction proceeds much faster in methanol than in acetonitrile. Moreover, an inverse kinetic isotope effect (KIE) is evidenced for the reaction in acetonitrile, which is attributed to a sterically congested transition state leading to the peroxo adduct. In methanol, however, no KIE is observed. A DFT analysis of the oxygenation reaction mediated by the μ-η²:η² peroxo core demonstrates that the major barrier after O_2 binding corresponds to electrophilic attack on the arene ring. The relevant orbital interaction occurs between the σ* orbital of the Cu_2O_2 unit and the HOMO of the ligand. On the basis of the activation energy for the rate-limiting step (18.3 kcal mol^{-1}) this reaction is thermally allowed, in agreement with the experimental observation. The calculations also predict the presence of a stable dienone intermediate which, however, escaped experimental detection so far. Reasons for these findings are considered. The implications of the results for the mechanism of tyrosinase are discussed.

Keywords: copper · hydroxylation · N ligands · O–O activation · reaction mechanisms

Introduction

Recent publication of the first crystal structure determination of a tyrosinase has opened a new perspective for understanding the chemical reactivity of this class of enzymes at a molecular level.[1,2] Tyrosinases (Ty) are ubiquitous copper enzymes mediating the hydroxylation of monophenols to *o*-diphenols and subsequent two-electron oxidation to *o*-quinones.[3] Specifically, tyrosine is converted to dopaquinone, the first step of melanine synthesis.[4] Two-electron oxidation of *o*-diphenols (catechols) to *o*-quinones is also catalyzed by the related enzyme catechol oxidase (CO), which, however, lacks monooxygenase activity.[5,6] The active sites of Ty and CO exhibit two copper atoms both of which are coordinated by three histidine residues (type 3 copper). The third group of proteins with type 3 copper active sites is that of hemocyanins (Hc), which serve as oxygen carriers in some arthropods and mollusks and exhibit highly cooperative oxygen-binding characteristics.[7]

There have been numerous attempts to reproduce and understand the chemical reactivity of tyrosinase with small-

[a] Dipl.-Chem. O. Sander, Priv. Doz. C. Näther, Prof. Dr. F. Tuczek
Institut für Anorganische Chemie
Christian Albrechts Universität Kiel
Max-Eyth Strasse 2, 24098 Kiel (Germany)
Fax: (+49) 431 880 1520
E-mail: ftuczek@uni-kiel.de

[b] Dipl.-Chem. A. Henß, Dipl.-Chem. C. Würtele, Prof. Dr. S. Schindler
Institut für Anorganische und Analytische Chemie
Justus-Liebig-Universität Gießen
Heinrich-Buff-Ring 58, 35392 Gießen (Germany)
Fax: (+49) 641 993 4149
E-mail: siegfried.schindler@chemie.uni-giessen.de

[c] Prof. Dr. M. C. Holthausen
Institut für Anorganische und Analytische Chemie
Johann Wolfgang Goethe-Universität Frankfurt
60438 Frankfurt am Main (Germany)
Fax: (+49) 798 294 17
E-mail: max.holthausen@chemie.uni-frankfurt.de

Supporting information for this article is available on the WWW under http://dx.doi.org/10.1002/chem.200800799.

molecule model systems, both on the basis of the hydroxylation or oxidation of external substrates and on hydroxylation of the ligand.[8,9,10,11] In the latter case part of the ligand coordinating one or both copper centers is hydroxylated after exposure of the Cu^I complex to dioxygen. The relevance of these reactions to tyrosinase has intensively been discussed, and a molecular mechanism of tyrosinase functionality has been suggested based on DFT calculations.[12,13] It has further been established that both aliphatic and aromatic parts of the ligand can be hydroxylated in this way (aliphatic and aromatic ligand hydroxylation).[8,14] The latter reactivity was discovered by Karlin and co-workers in their study on $[Cu_2(XYL)]$ (XYL = tetrakis[2-(pyridin-2-yl)ethyl]benzene-1,3-diamine).[15] Reaction of the Cu^I_2 precursor with O_2 was found to lead to hydroxylation of the bridging xylylene spacer in the 2-position. It was later shown that the Cu^I_2 species binds O_2 in a side-on bridging fashion and that most probably the Cu_2 μ-η^2:η^2-peroxo unit mediates electrophilic attack on the aromatic ring, leading to O–O cleavage and hydroxylation.[16] A mechanistic alternative to this scenario is full or partial conversion of the Cu^{II}_2 μ-η^2:η^2 peroxo species to the Cu^{III}_2 bis(μ-oxo) form, which then mediates the aromatic hydroxylation reaction.[17] For the $[Cu_2(XYL)]$ complex, this pathway has been excluded. For other systems, however, aromatic ligand hydroxylation mediated by a Cu_2 bis(μ-oxo) species is well established.[18]

A simplified version of the Karlin system is provided by Cu^{II} bis(imine) complexes, which also mediate hydroxylation of the bridging ligand on reaction with O_2. This reaction has been intensively studied as well,[19,20,21,22] and its relevance to the tyrosinase reaction has been stressed.[23,24] The binucleating ligand contains a bridging xylylene group carrying two arms which provide two nitrogen donors (one imine and one terminal amine) each. On exposure of the Cu^I precursor to dioxygen, the central phenylene spacer is hydroxylated, in analogy to the XYL complex (Scheme 1). In the latter system, however, the bis(imine) ligation enforces an almost planar molecular geometry, which highly restricts the configuration space involved in the ligand hydroxylation reaction. Although it has been speculated that in this reaction a peroxo or bis(μ-oxo) intermediate is involved, no such intermediate has ever been detected. Accordingly, key features of the reaction course for this important class of tyrosinase model systems have remained unclear to date.

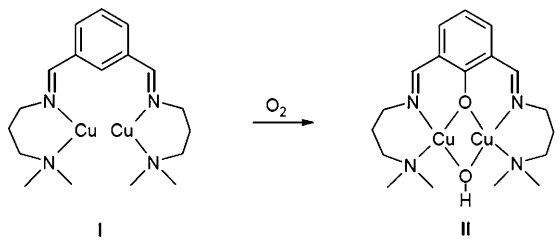

I II

Scheme 1. Hydroxylation of the Cu_2(DAPA) core of **I** leading to product **II** (charges are omitted).

Herein we present spectroscopic, kinetic, and theoretical investigations on the Cu_2 bis(imine) complex $[Cu_2(DAPA)]^{2+}$ (**I**; DAPA = 1,3-bis-[(3-(*N*-dimethyl)propyl)iminomethyl]benzene; Scheme 1) with the goal of developing a mechanistic scenario for the ligand hydroxylation reaction occurring in this system. To this end the kinetics of the reaction were studied in different solvents and at different temperatures, and a deuterium-substituted ligand was also employed. In order to monitor the time course of the hydroxylation spectroscopically the UV/Vis spectra of the Cu^I precursor **I** and the hydroxylated Cu^{II} product **II** were analyzed and compared with each other. Moreover, the vibrational spectroscopic properties of the reactant and the product were determined. In particular, the IR and Raman spectra of the Cu^{II} complex **II** are analyzed with the help of ^{18}O substitution and quantum chemical calculations. Reactant **I** and product **II** were further characterized by X-ray crystallography. Density functional theory was employed to identify potential reaction pathways leading from the initially formed μ-η^2:η^2 peroxo dicopper intermediate to the hydroxylated product **II**. The quantum chemical results are discussed in light of the experimental findings, and implications for the reactivity of tyrosinase are considered.

Experimental and Computational Details

Materials and techniques: The reagents isophthalaldehyde and 3-dimethylaminopropylamine were used as received from Aldrich Chemical Co. Tetrakis(acetonitrile)copper(I) hexafluorophosphate was either obtained commercially from Aldrich or synthesized from copper(I) oxide according to a method described in the literature.[25] Solvents used were all of reagent grade and were further purified by refluxing over drying agents and distilling under argon. Methanol was distilled from $Mg(OCH_3)_2$, diethyl ether from $LiAlH_4$, and acetonitrile from CaH_2. The NMR spectra were recorded at 300 K on a Bruker Avance 400 Pulse Fourier Transform spectrometer operating at a ^1H frequency of 400.13 MHz and ^{13}C frequency of 100.62 MHz relative TMS as standard. Elemental analysis was performed using an Euro Vector CHNS-O element analyzer (Euro EA 3000). Samples were burned in sealed tin containers in a stream of oxygen. FTIR spectra were recorded in KBr pellets on a Mattson Genesis Type I spectrometer. Optical absorption spectra of solutions were recorded on a Cary 5 UV/Vis/NIR spectrometer equipped with a CTI cryocooler. Raman spectra were recorded on a Bruker IFS 66 FT spectrometer equipped with a Raman assembly.

Variable-temperature stopped-flow measurements allowed the collection of time-resolved UV/Vis spectra for the fast reaction of **I** with dioxygen in methanol. Solutions of the complexes were prepared in a glove box (MBraun, Garching, Germany) and transferred by syringe to the low-temperature stopped-flow instrument. A dioxygen-saturated solution was prepared by bubbling dioxygen through methanol in a syringe (solubility of dioxygen in MeOH at 25 °C: 8.5 mM).[26] Lower dioxygen concentrations were obtained by mixing these solutions with argon-saturated solvents. The reaction was studied under pseudo-first-order conditions ($[complex] \ll [O_2]$), and time-resolved UV/Vis spectra of the reactions of dioxygen with copper(I) complexes were recorded with a modified Hi-Tech SF-3L low-temperature stopped-flow unit (Salisbury, UK) equipped with a J & M TIDAS 16-500 photodiode-array spectrophotometer (J & M, Aalen, Germany). Data fitting was performed with the integrated J & M software Kinspec. Details of such studies have been described previously.[27]

Single-crystal structure analysis: The X-ray crystallographic data for complex **I** were collected at 173 K on a STOE IPDS diffractometer equipped

with a low-temperature system (Karlsruher Glastechnisches Werk). $Mo_{K\alpha}$ radiation ($\lambda = 0.71069$ Å) and a graphite monochromator were used. Cell parameters were refined by using up to 5000 reflections. No absorption corrections were applied. The structure was solved by direct methods with SHELXS97, and refined as a racemic twin by using full-matrix least-squares techniques in SHELXL97 (BASF parameter: 0.542). An attempt to solve and refine the structure in the centrosymmetric space group $P2_1/m$ was unsuccessful. The hydrogen atoms were positioned geometrically and all non-hydrogen atoms were refined anisotropically, if not mentioned otherwise. Details of the structure determination are given in Table 1.

Table 1. Crystal data and structural refinement for **I** and **II**.

Parameter	**I**	**II**
empirical formula	$C_{24}H_{39}N_7Cu_2P_2F_{12}$	$C_{19}H_{32}N_4Cu_2Cl_4O_{10}$
formula weight	842.64	745.37
temperature [K]	173(2)	170(2) K
crystal system	monoclinic	triclinic
space group	$P2_1$	$P\bar{1}$
wavelength [Å]	0.71073	0.71073
a [Å]	11.491(2)	7.8818(9)
b [Å]	25.391(5)	13.955(2)
c [Å]	12.564(3)	14.649(2)
α [°]		62.06(2)
β [°]	105.59(3)	$\beta = 84.90(2)$
γ [°]		81.66(2)
V [Å^3]	3530.8(12)	1407.9(3)
Z	4	2
ρ_{calcd} [Mg m^{-3}]	1.585	1.758
abs. coeff. [cm^{-1}]	1.386	1.948
crystal size [mm]	$0.25 \times 0.1 \times 0.12$	$0.2 \times 0.2 \times 0.1$
θ range for data collection [°]	2.13–26.04	2.61–25.03
index ranges	$-14 \le h \le 13$, $-31 \le k \le 31$, $-14 \le l \le 15$	$-9 \le h \le 9$, $-16 \le k \le 16$, $-17 \le l \le 17$
reflns collected	24832	12085
independent reflns	13443	4681
reflns with $I > 2\sigma(I)$	6125	3304
R_{int}	0.1061	0.1250
GOF on F^2	0.780	0.998
$R1$ [$I > 2\sigma(I)$]	0.0532	0.0519
$wR2$ [$I > 2\sigma(I)$]	0.0845	0.1172
$R1$ (all data)	0.1389	0.0805
$wR2$ (all data)	0.1065	0.1319
max./min. residual electron density [e Å^{-3}]	0.489/−0.324	0.646/−1.242

Data collection on complex **II** was performed with an Imaging Plate Diffraction System (IPDS-1) from STOE & CIE. Structure solution was done with SHELXS-97, and structure refinement against F^2 with SHELXL-97. All non-hydrogen atoms were refined with anisotropic displacement parameters. All CH hydrogen atoms were positioned with idealized geometry and were refined isotropically by using a riding model. The OH H atom was located in the difference map; its bond length was set to ideal values and afterwards it was refined by using a riding model. CCDC-686492 (**I**) and CCDC-686493 (**II**) contain the supplementary crystallographic data for this paper. These data can be obtained free of charge from The Cambridge Crystallographic Data Centre via www.ccdc.cam.ac.uk/data_request/cif.

Tetrakis(acetonitrile)copper(I) perchlorate: $CuCO_3$ was added to perchloric acid (10 mL) until the solution was saturated. The remaining precipitate was filtered off and the solution was concentrated in vacuo. After cooling the solution overnight, blue crystals precipitated, which were filtered off and dissolved in acetonitrile. The blue solution was refluxed with copper turnings under argon till the color disappeared. After cooling of the colorless solution colorless crystals precipitated, which were filtered off and dried. Elemental analysis (%) calcd for $CuC_8H_{12}N_4ClO_4$: C 29.37, H 3.7, N 17.12, Cl 10.84; found: C 29.2, H 3.66, N 17.4, Cl 10.81.

1,3-bis{[3-(*N*,*N*-dimethyl)propyl]iminomethyl}benzene (DAPA): Isophthalaldehyde (400 mg, 2.98 mmol) and (610 mg, 5.96 mmol) 3-dimethylaminopropylamine were dissolved in methanol (40 mL) and the solution heated to reflux for 1 h. The solvent was removed on a rotary evaporator and the remaining yellow oil dried in vacuo. The product was purified by chromatography on silica gel with methanol as eluant ($R_f = 0.4$). Elemental analysis (%) calcd for $C_{18}H_{30}N_4$: C 71.48, H 10.0, N 18.52; found: C 70.93, H 10.35, N 18.53; ^{1}H NMR (400 MHz, CD_2Cl_2/TMS): $\delta = 8.3$ (s, 2H; imine H), 8.03 (s, 1H; ArH), 7.76 (dd, 2H; ArH), 7.44 (t, 1H; ArH), 3.61 (dt, 4H, $=NCH_2$), 2.3 (t, 4H; $-CH_2N$), 2.18 (s, 12H; CH_3), 1.81 ppm (q, 4H; $-CH_2-$); ^{13}C NMR (100.6 MHz, CD_2Cl_2/TMS): $\delta = 160.2$, 137.0, 129.6, 128.7, 127.5, 59.4, 57.4, 42.2, 29.0 ppm; MS (EI, 70 eV): m/z (%): 303.4 (100) [M^+]; calcd: 303.46.

$[Cu^I_2(DAPA)(CH_3CN)]^{2+}$ (I): The complex was prepared under argon atmosphere, either according to the published procedure as the PF_6 salt (**Ia**)[28] or as the ClO_4 salt (**Ib**) by using the following modified procedure: DAPA (230 mg, 0.76 mmol) was dissolved in dry, degassed methanol (20 mL). Tetrakis(acetonitrile)copper(I) perchlorate 296 mg (1.52 mmol) was added. The resulting yellow solution was heated for 1 h. After concentrating the solution to 10 mL a yellow solid precipitated, which was filtered off and washed with degassed methanol (2×5 mL). ^{1}H NMR (400 MHz, CD_3CN/TMS): $\delta = 8.37$ (s, 2H, imine H), 8.25 (s, 1H, ArH), 7.93 (d, 2H, ArH), 7.55 (t, 1H, ArH), 3.72 (t, 4H, $=NCH_2$), 2.51 (t, 4H, $-CH_2N$), 2.23 (s, 12H, CH_3), 1.81 ppm (q, 4H, $-CH_2-$); ^{13}C NMR (100.6 MHz, CD_3CN/TMS): $\delta = 163.2$, 137.0, 131.8, 130.0, 129.1, 62.7, 60.7, 47.2, 29.3 ppm. Crystals suitable for diffraction studies were obtained by diffusion of diethyl ether into a solution of **Ia** in acetonitrile.

Synthesis of the tetraphenylborate salt of $[Cu^I_2(DAPA)]$ (**Ic**): Salt **Ib** (200 mg, 0.32 mmol) was dissolved in dry, degassed acetonitrile (10 mL). Potassium tetraphenylborate (228 mg, 0.64 mmol) dissolved in acetonitrile (15 mL) was added. After concentrating the yellow solution to 10 mL a colorless solid precipitated and was filtered off. The solution was evaporated to dryness and the yellow residue was used without further purification. The conversion of the perchlorate to the tetraphenylborate salt was checked for completeness by IR spectroscopy. The perchlorate bands were absent in the product.

$[Cu^{II}_2$-(DAPA-O)(OH)] (II), perchlorate salt: Salt **Ib** (60 mg) was dissolved in dry dichloromethane (40 mL). Dioxygen was bubbled through the solution for 5 min. The color changed from yellow to green. The solution was concentrated to 5 mL. On adding 20 mL of diethyl ether a green solid precipitated, which was filtered off. The product was recrystallized from dichloromethane by diffusing diethyl ether into the solution. Green crystals were obtained. Elemental analysis (%) calcd for $C_{18}H_{30}N_4Cu_2O_2(ClO_4)_2(CH_2Cl_2)$: C 30.6, H 4.33, N 7.52; found: C 31.1, H 4.78, N 7.63; UV/Vis (CH_3CN) λ_{max} (ε) = 255 (35753), 357 (9135), 628 nm (253 M^{-1} cm^{-1}). The ^{18}O isotopomer of **II** was prepared analogously by employing $^{18}O_2$ instead of $^{16}O_2$.

[D_6]Isophthalaldehyde: m-[D_{10}]xylene 2.5 g (21.55 mmol) was dissolved in CCl_4 (250 mL). *N*-Bromosuccinimide (22.55 g, 126.7 mmol) and one drop of bromine were added. The reaction was started with small amounts of 2,2′-azobisisobutyronitrile and the mixture was heated for 15 h under reflux. The succinimide was filtered off and after removal of the solvent the product was used without further purification. The reddish product was dissolved in H_2SO_4 (30 mL) at 110 °C. After the formation of bromine the solution was hydrolyzed with ice (100 mL) and extracted with methyl *tert*-butyl ether (MTBE). The combined organic phases were neutralized with $NaHCO_3$ solution and the aqueous phase was again extracted with MTBE. The combined organic phases were dried over $MgSO_4$ and after removal of the solvent the product was purified by chromatography on silica gel with dichloromethane as eluant ($R_f = 0.35$). ^{1}H NMR showed no signals; ^{13}C NMR (100.6 MHz, CD_2Cl_2/TMS): $\delta = 190.7$ (deutero-t), 136.9 (s), 134.1 (deutero-t), 130.2 (deutero-t), 129.4 ppm (deutero-t); MS (EI, 70 eV): m/z (%): 141.1 (100) [M^+]; calcd: 141.2.

$[Cu^{I}_2([D_6]DAPA)(CH_3CN)_3](ClO_4)_2$ (I^D): [D_6]Isophthalaldehyde (0.4 g, 2.82 mmol) was dissolved in dry methanol (40 mL). 3-Dimethylaminopropylamine (0.75 mL, 5.9 mmol) was added and the solution heated to reflux for 1 h. After cooling tetrakis(acetonitrile)copper(I) perchlorate (1.1 g, 5.9 mmol) was added to the orange solution, which was stirred for 1 h. After concentrating the solution to 10 mL, a yellow solid precipitated, which was filtered off and washed with degassed methanol (2×5 mL). ^{1}H NMR (400 MHz, CD_3CN/TMS): $\delta = 3.74$ (t, 4H, $=NCH_2$), 2.53 (t, 4H; $-CH_2N$), 2.24 (s, 12H; CH_3), 1.82 ppm (q, 4H; $-CH_2-$); ^{2}H NMR (61.4 MHz, CD_3CN/TMS) between 7.4 and 8.4 ppm four peaks with integration ratio 2:2:1:1 were observed; ^{13}C NMR (100.6 MHz, CD_3CN/TMS): $\delta = 61.8$, 59.8, 46.2, 28.2 ppm.

$[Cu^{II}_2([D_6]DAPA\text{-}O)(OH)]$, perchlorate salt ($II^D$): Salt I^D (60 mg) was dissolved in dry dichloromethane (40 mL). Dioxygen was bubbled through the solution for 5 min. The color changed from orange to green. The solution was concentrated to 5 mL. By adding diethyl ether (20 mL), a green solid precipitated which was filtered off and recrystallized from dichloromethane. Elemental analysis (%) calcd for $C_{18}H_{12}D_6N_4Cu_2O_2(ClO_4)_2$: C 32.44, H 5.44, N 8.41; found: C 32.92, H 5.28, N 8.20.

Caution! Although the compounds reported in this paper seem to be stable to shock and heat, extreme care should be used in handling them because of the potential explosive nature of perchlorate salts.

Computational methods: Quantum-chemical calculations on reaction pathways were performed at the DFT level with the three-parameter hybrid functional B3LYP/G[29] as implemented in the ORCA program.[30] Geometry optimizations and harmonic frequency calculations were performed by employing the SVP basis set of Ahlrichs and co-workers[31] for all atoms. In all calculations we used the TightSCF, NoFinalGrid, and Grid4 options/cutoffs, and the RIJONX approach[32] was used together with the SV/J auxiliary basis set[33] for enhanced numerical efficiency via the RI approximation.[34] Solvation effects were included in these calculations by employing the COSMO continuum model (solvent acetonitrile, dielectric constant at room temperature $\varepsilon = 36.6$; the following radii were used for construction of the cavity: H: 1.300, C: 2.000, N: 1.830 Å, O: 1.720, Cu: 2.223, solvent: 1.300 Å).[35] The nature of stationary points localized (minima or transition structures) were identified by Hessian calculations based on numerical evaluation of energies and analytical gradients, which were also used to obtain zero-point vibrational energy (ZPVE) and thermal contributions to Gibbs free energies at 298.15 K. We verified the connections between minima and transition structures implied in Figure 12 below by intrinsic reaction coordinate (IRC) calculations. For transition-state searches, IRC calculations, and numerical Hessian calculations we used the Gaussian 03[36] external driver facility in combination with a Gau_External module that we developed to extract energies and gradients from ORCA calculations, which were then fed into geometry optimization driver routines of the Gaussian 03 program.[37] Improved final energies were obtained by single-point calculations employing the B3LYP/G functional in combination with the TZVP basis of Ahlrichs and co-workers and the COSMO continuum solvent model (together with the TZV/J auxiliary basis sets, with all other program parameters and options as described above).

In several instances frequency analyses of stationary points obtained for the full molecular model showed spurious imaginary modes related to rotation of the methyl groups at the *tert*-amine N donor atoms, which seriously affects the use of computed ZPVE and thermal contributions to obtain Gibbs free energies. In view of the unjustifiably large numerical effort necessary for repeated reoptimizations of geometries and numerical frequency calculations, we decided to perform investigations on reaction pathways based on a simpler molecular model, in which we replaced the methyl groups by hydrogen atoms.

In all species studied here (but **TS8** with its closed-shell singlet ground state wave function, see Figure 12 below and Table S1, Supporting Information), the presence of two coupled Cu^{II} ions with their formal d^9 electronic configuration gives rise to spin–spin coupling phenomena, that is, the two unpaired electrons can couple to yield singlet or triplet states. While treatment of the triplet states is straightforward within the spin-unrestricted Kohn–Sham framework, a description of the corresponding singlet states by spin-restricted Kohn–Sham calculations can be highly problematic, depending on the strength of the spin–spin coupling. The broken-symmetry (BS) approach has been identified as an efficient means to include the dynamic and static correlation effects underlying these magnetic interactions to a large extent, and it has been applied to related bioinorganic problems with considerable success.[38] Following the suggestion of Noodleman et al.[39] we applied spin-unrestricted broken-symmetry calculations for the antiferromagnetically coupled singlet states. The overlap integrals $\langle\alpha|\beta\rangle$ of the magnetic orbitals obtained for the BS wave functions vary significantly (Table S1, Supporting Information), which indicates strongly varying coupling strengths between the spin centers involved. We therefore applied the formalism of Yamaguchi et al.[40] to obtain the Heisenberg coupling parameter J related to the phenomenological Heisenberg Hamiltonian $H = -2JS_AS_B$ [Eq. (1)].

$$J = -\frac{E_{HS} - E_{BS}}{\langle S^2\rangle_{HS} - \langle S^2\rangle_{BS}} \quad (1)$$

This approach covers the range from weak to strong coupling situations. The BS wave functions were obtained by employing the corresponding orbital transformation procedure implemented in ORCA.[41] In the present context, a negative value for J corresponds to an "antiferromagnetically coupled" or "open-shell" singlet ground state.

For some species involved in the reaction pathways discussed below we found triplet ground states ($J = +25$ to $+534$ cm^{-1}, see Table S1, Supporting Information). In some instances we reoptimized the corresponding triplet structures, but we did not observe any significant energy lowering or structural change (e.g., 1 kcal mol^{-1} in the case of **1** with essentially unaltered structural features). Analysis of spin densities for all species investigated revealed that all magnetic interactions are caused by interactions of spin densities essentially localized on the copper ions with their formal d^9 electronic configurations. These Cu^{II}-based spin systems exhibit antiferromagnetically coupling in most cases, which gives rise to singlet ground states, but triplet ground states result in some instances as a consequence of ferromagnetic spin coupling. The intricacies of magnetic coupling in related Cu_2O_2 systems due to the interplay between electronic and structural properties are the subject of ongoing research,[42] and, in view of the general tendency of the B3LYP functional to overestimate the stability of high-spin over low-spin states for transition metal ions,[43] they are outside the scope of the present study. The small energy differences between singlet and triplet species documented in Table S1 (<2 kcal mol^{-1} in all cases) are insignificant in the context of our investigation of reaction pathways. Hence, for the present system we can safely exclude the possibility that copper-based spin coupling gives rise to a prominent two-state reactivity scenario[44] in the sense that spin crossover phenomena could provide alternative reaction pathways that significantly alter the mechanistic scenario proposed below.[45]

Additional calculations were performed to support analysis of experimental IR and resonance-Raman spectra. Here we used the UBP86 functional[46] to optimize (BS) the singlet structure for the full molecular model of the hydroxylated product, starting from the X-ray structure of **II**. It is well established that this level of DFT quite generally provides vibrational frequencies in good agreement with experimentally determined spectra.[47,48] Calculated frequencies were therefore used without further scaling.

Results

X-ray structure analysis

*Cu^I complex **Ia***: The DAPA ligand and the corresponding copper complex were prepared according to the literature.[25] Despite the facile synthesis of **I** and related bis(imine) complexes, crystallographic characterizations of these compounds are rare. Recently a copper(I) complex with a ligand similar to DAPA (ethylene instead of propylene bridges)

was structurally characterized, but in this case a dinuclear complex with a Cu^{I}:ligand ratio of 2:2 was obtained.[49] After optimizing conditions in our crystallization experiments we succeeded in obtaining crystals of $[Cu^{I}_{2}(DAPA)(CH_3CN)_3](ClO_4)_2$ (**Ia**). The molecular structure of the complex cation is shown in Figure 1.

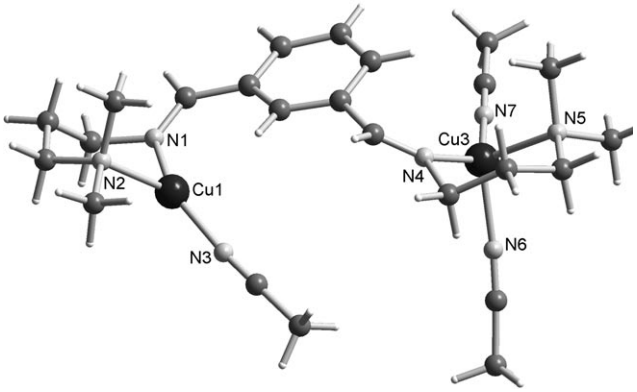

Figure 1. Molecular structure of the cation of **I**. Selected bond lengths [Å] and angle [°]: Cu1–N3 1.85(1), Cu1–N1 1.96(9), Cu1–N2 2.055(8), Cu3–N7 1.96(1), Cu3–N6 2.02(1), Cu3–N4 2.019(9), Cu3–N5 2.11(1); Cu3-Cu1-N1 138.9(3).

Compound **Ia** crystallizes in the monoclinic space group $P2_1$ with two complex cations and four anions per unit cell. The two copper(I) centers are bridged by a *m*-xylyl group with a Cu1···Cu3 separation of 7.1(1) Å. Each copper ion is coordinated by one imine nitrogen atom (N1/N4) and one aliphatic amine nitrogen atom (N2/N5) per bidentate DAPA arm. As additional coligands one or two acetonitrile molecules are ligated to the copper ions. One N-bonded MeCN molecule completes the almost trigonal-planar coordination geometry of Cu1. With two bound acetonitrile molecules the coordination geometry around Cu3 is best described as distorted tetrahedral. The formation of six-membered chelate rings leads to respective N1-Cu1-N2 and N4-Cu3-N5 angles of 96.7(3) and 95.2(3)° which substantially deviate from ideal trigonal or tetrahedral geometry. The dihedral angle between the N1-Cu1-N2 and N4-Cu3-N5 planes is 53.09°. As expected, the Cu–N bond lengths of the tricoordinate Cu1 center are shorter than that of Cu3 (see Supporting Information). The "harder" amine nitrogen atoms N2 and N5 are bound more weakly to the copper(I) ion than the imine nitrogen atoms N1 and N4.

Feringa and co-workers have reported the synthesis and characterization of a structurally related binuclear Cu^{I} complex, in which each copper center is coordinated to one bidentate ligand arm and one acetonitrile molecule.[50] Comparison of this crystal structure with that of **Ia** reveals quite similar Cu–N bond lengths, all in the range typical for three-coordinate Cu^{I} complexes,[50,51] while the two complexes differ in the bond angles around the copper ions because of their different donor-atom environments (aliphatic amine versus pyridine nitrogen donor atoms). A larger chelate ring size and a different Cu-to-ligand ratio are also responsible for significant differences in bond lengths and angles between **Ia** and a binuclear Cu^{I} Schiff base complex characterized recently by Mukherjee and co-workers.[49] Furthermore, comparison of **I** with a related dinuclear macrocyclic Schiff base copper(I) complex previously described by Utz et al. as well as by Rieger and co-workers also shows differences in bond lengths and angles around the tetracoordinate Cu3 center of **I**.[21,52] Most likely this is a consequence of the macrocyclic ligand, which enforces a bowl shape of the complex, and compared to **I** it has a much smaller Cu···Cu separation of 4.250(3) Å. Dinuclear copper(I) complexes of the nonmacrocyclic ligand derivative have been described recently, but for these no hydroxylation reactions were observed.[53]

*Cu^{II} complex **II***: Oxygenation of the Cu^{I} precursor **Ib** in dichloromethane leads to the Cu^{II}_{2} complex **II**. Single crystals suitable for X-ray analysis were obtained by diffusion of diethyl ether into a solution of **II** in dichloromethane. The structure of the complex is shown in Figure 2. Compound **II** crystallizes in the triclinic space group $P\bar{1}$ with $Z=2$ and all atoms in general positions. Each of the two crystallographically independent copper atoms is coordinated by two nitrogen atoms and one oxygen atom of the ligand as well as one hydroxyl oxygen atom within a strongly distorted square-planar geometry (Figure 2). There are two additional contacts to oxygen atoms of perchlorate anions of 2.4497(4) Å (Cu1–O11) and 2.6724(3) Å (Cu2–O13). If these contacts are taken into account the coordination around the copper atoms can be described as strongly distorted octahedral. In **II** the copper atoms are connected by the perchlorate anions to form chains which extend in the direction of the crystallographic *a* axis.

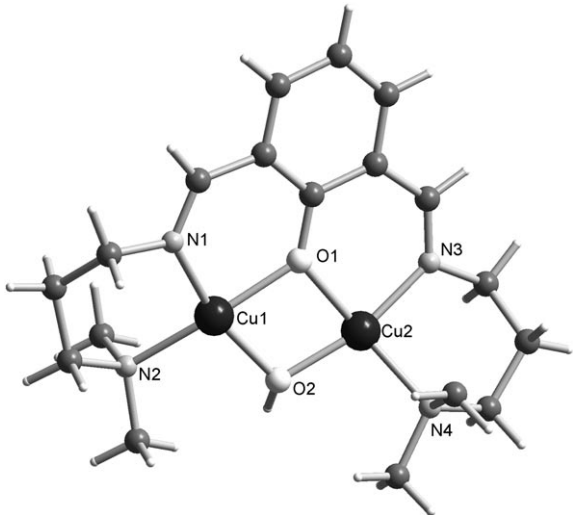

Figure 2. Molecular structure of the cation of **II**. Selected bond lengths [Å] and angles [°]: Cu1–O2 1.899(3), Cu1–O1 1.986(4), Cu2–O2 1.899(4), Cu2–O1 1.991(3), Cu1–Cu2 3.0546(11), O1–C1 1.324(6), Cu1–N1 1.938(4), Cu1–N2 2.025(5), Cu2–N3 1.948(5), Cu2–N4 2.031(4); N1-Cu1-N2 95.13, N3-Cu2-N4 97.8, Cu1-O1-Cu2 100.39, Cu2-O2-Cu1 107.07.

Evidently the phenyl ring of the bis(imine) ligand has been hydroxylated on the reaction of **Ib** with O_2 to form a phenoxo group that bridges the two Cu^{II} centers; a second bridge is provided by a hydroxo ligand. The μ-hydroxo μ-phenoxo Cu_2 unit is coordinated by the two terminal amine and two imine nitrogen atoms of the bis(imine) ligand to give an almost perfectly planar dinuclear complex with square-planar coordination of each Cu^{II} center. The Cu···Cu distance is 3.055 Å and the average Cu···N distances are 1.94 Å for the imine nitrogen atoms (N1 and N3) and 2.03 Å for the amine nitrogen atoms (N2 and N4). Similar to the Cu^{I} complex the N1-Cu1-N2 and N3-Cu2-N4 angles are 95.1(3) and 97.8°, due to formation of a six-membered chelate ring. As expected, the molecular structure of **II** is very similar to that of this complex published by Drew et al.[28] The Cu···Cu distance in **II** is slightly longer (3.055 instead of 3.015 Å), most likely as a consequence of the water molecule that is additionally coordinated to CuB in the complex of Drew et al. Moreover, two perchlorate anions are coordinated at about 2.5 Å (vide supra).

Spectroscopic investigations

UV/Vis spectroscopy: The UV/Vis spectrum of **II** in acetonitrile is shown in Figure 3. It exhibits two intense bands in the region between 200 and 300 nm and one band at 357 nm ($\varepsilon = 10000\,M^{-1}\,cm^{-1}$) The latter feature is absent in the spectrum of Cu^{I} precursor **I**, which only shows a rising slope below 300 nm with a couple of weak shoulders. The 357 nm band is therefore the most conspicuous UV/Vis spectroscopic signature of the oxygenated complex. It has been assigned to a charge-transfer transition from the Cu^{II} centers to the hydroxylated bis(imine) ligand.[22] At higher concentration a weak absorption band can also be detected at 663 nm, which is assigned to a ligand-field transition of the square-planar Cu^{II} centers. Oxygenation of **I** to **II** proceeds only slowly in acetonitrile (see below); therefore, we employed methanol as solvent as well. Figure S1 (Supporting Information) shows the spectra of **I** and **II** in methanol; the spectrum of **II** was obtained after bubbling O_2 through a solution of **I**. As in the spectrum of **II** in acetonitrile, an intense band is observed at 360 nm and a ligand-field band at 700 nm.

Vibrational spectroscopy: Infrared and Raman spectra of **I** and **II** were obtained from solid samples at room temperature and are presented in Figure 4–7. We also studied the ^{18}O isotopomer of **II**, which was prepared by reaction of **I** with $^{18}O_2$. Spectral assignments were facilitated by comparison with computed harmonic frequencies at the UBP86/SVP level, which show an overall pleasing agreement with the experimental results (Figure 5). In contrast to our initial expectation $^{16}O/^{18}O$ isotopic substitution in **II** does not lead to the identification of a unique vibrational signature for a C–O stretching vibration. Detailed analysis of the computed spectra reveals instead that there are several normal modes with varying C–O stretching contributions. Here we report

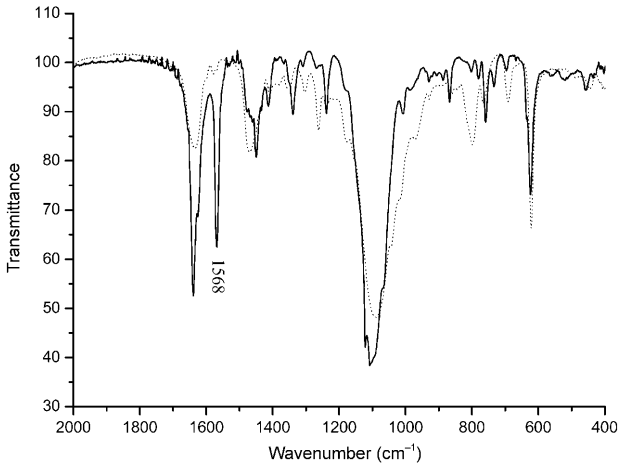

Figure 4. IR spectra of **Ib** (dotted) and **II** (solid).

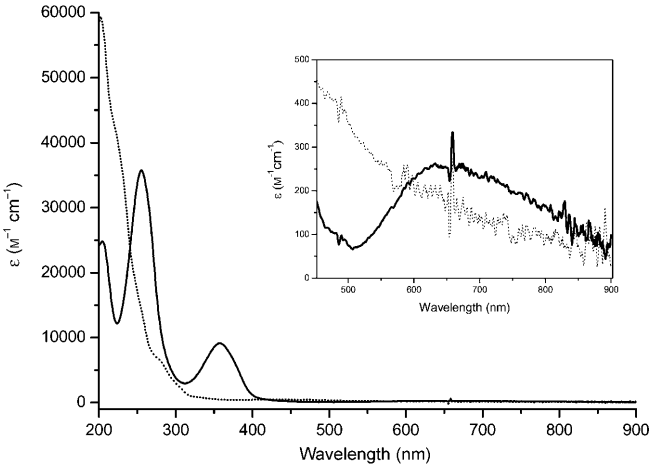

Figure 3. UV/Vis spectra of **Ib** (dotted line, $8\times10^{-5}\,mol\,L^{-1}$) and **II** (solid line, $11\times10^{-5}\,mol\,L^{-1}$) in acetonitrile.

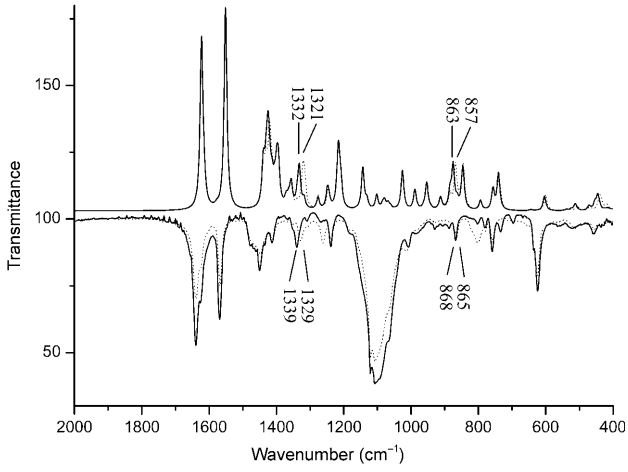

Figure 5. Experimental (bottom) and calculated (top) IR spectra of **II** (solid lines) and $^{18}O_2$-**II** (dotted lines) with isotope-sensitive bands.

only assignments of the most prominent vibrational features as a result of a careful correlation between measured and computed spectra. Figure 8 shows dominant atomic contributions to normal modes for the vibrations discussed below.

The IR (Figure 4 and Figure 5) and Raman (Figure 6 and Figure 7) spectra of **I** and **II** show an intense signal at 1630 cm^{-1} which correlates with a normal mode in the computed spectra dominated by the symmetric stretching motion of the Schiff base C=N bonds (1622 cm^{-1}, see Figure 8); this band exhibits a second feature due the corresponding antisymmetric vibration (computed at 1615 cm^{-1}, not shown in Figure 8) with much lower intensity. On oxygenation of **I** an intense band appears in the spectrum of **II** at 1568 cm^{-1} (Figure 4). This band corresponds to a vibration at 1551 cm^{-1} in the computed spectrum (Figure 8) and can be assigned to an asymmetric deformation mode in the aromatic ring in **II**. As consistently revealed by both experimental and computed spectra, neither band shows any C–O participation. Buried among a series of bands between 1443 and 1394 cm^{-1} due to C–H stretching and bending vibrations of all parts of the ligand, the computed spectra exhibit an intense peak at 1424 cm^{-1} (shifted to 1420 cm^{-1} on ^{18}O substitution) that contains some C–O stretching component. In the experimental spectra this signal occurs on oxygenation of **I** at 1450 cm^{-1} (Figure 4) but does not show any significant isotopic shift in the spectrum of ^{18}O-**II**. One band at 1357 cm^{-1} in the spectrum of **I** moves to 1339 cm^{-1} in the spectrum of **II**. Comparison of the IR spectra of ^{16}O-**II** and ^{18}O-**II** (Figure 5) reveals a significant ^{18}O shift of this mode from 1339 cm^{-1} in ^{16}O-**II** to 1329 cm^{-1} in the spectrum of ^{18}O-**II**. Almost the same isotopic shift (11 cm^{-1}) is found in the computed spectra (1332 $cm^{-1}\rightarrow$1321 cm^{-1}), in line with a significant C–O contribution to this normal mode (see Figure 8). A lower-energy band at 866 cm^{-1} shifts to 861 cm^{-1} on isotopic substitution. This is reproduced by a computed vibration at 863 cm^{-1} which shifts to 857 cm^{-1} and involves significant O motion (see Figure 8).

The FT Raman spectra of **I** and **II** obtained with $\lambda_{exc}=$ 1064 nm are shown in Figure 6. A comparison of the FT Raman spectra of ^{16}O-**II** and ^{18}O-**II** (Figure 7) reveals only small isotopic shifts. After oxygenation of **I** two prominent new peaks appear at 1450 and 1257 cm^{-1}, but only the latter has some minor C–O contribution: In the region around 1250–1280 cm^{-1}, where normally the (phenolate) C–O stretching vibration is found,[16,54] only the intense peak at 1257 cm^{-1} shifts to 1254 cm^{-1} upon ^{18}O substitution, and DFT calculations indeed reveal some minor contribution from the C–O stretch to this vibration (1249$\rightarrow$1247 cm^{-1}; not shown in Figure 8). Three less intense peaks with small isotope shifts are observed at 1313 cm^{-1} (shifting to 1308 cm^{-1}), 1330 cm^{-1} (shifting to 1327 cm^{-1}) and 1371 cm^{-1} (shifting to 1366 cm^{-1}). The lowest-energy band may correspond to the vibration calculated at 1317 cm^{-1}, shifting to 1315 cm^{-1} (see Figure 8).

To conclude, the only vibration with a strong isotope shift (−10 cm^{-1}) is located at 1339 cm^{-1} (exptl; calcd: 1332 cm^{-1}) and has mostly IR intensity. It has the most prominent C–O contribution in the spectral range investigated. Some other vibrations show minor isotope shifts on the order of −3 to −5 cm^{-1}, depending on the contribution of the C–O stretching motion.

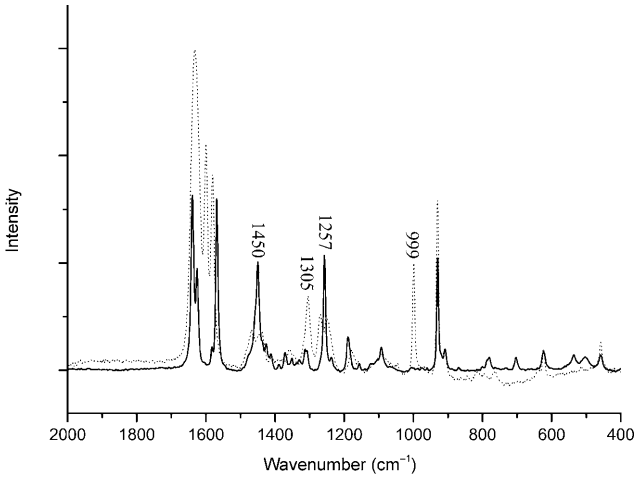

Figure 6. FT Raman spectra of **Ib** (dotted line) and **II** (solid line).

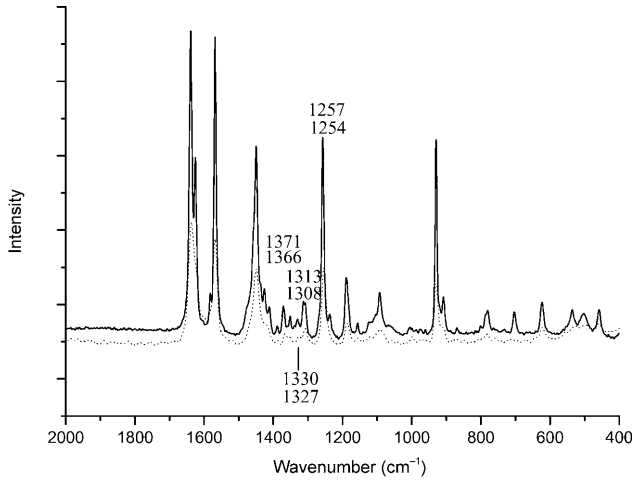

Figure 7. FT Raman spectra of **II** (solid line) and ^{18}O-**II** (dotted line).

Kinetic investigations: Yellow solutions of **Ia** in methanol turn immediately green when exposed to dioxygen with formation of **II**. Time-resolved spectra could be obtained by low-temperature stopped-flow techniques; a typical example of the oxidation reaction in methanol is shown in Figure 9. The spectra resemble those obtained previously by some of us in kinetic studies on the related imine systems $[Cu_2(HBPB\text{-}H)(CH_3CN)_2](BF_4)_2$ and $[Cu_2mac(CH_3CN)_2](ClO_4)_2$ (HBPB = 1,3-bis[*N*-(2-pyridylethyl)formimidoyl]benzene; mac = 3,6,9,17,20,23-hexaazatricyclo[2.3.3.1.1]triaconta-1(29),2,9,11(30),12(13),14,16,23,25,27-decaene).[27] Again, similar to these systems, we could not detect the buildup of a dioxygen adduct. This is in contrast to the complex $[Cu_2(XYL)]$ reported by Karlin and co-workers, for which spectroscopic detection of such an intermediate was possible at low tem-

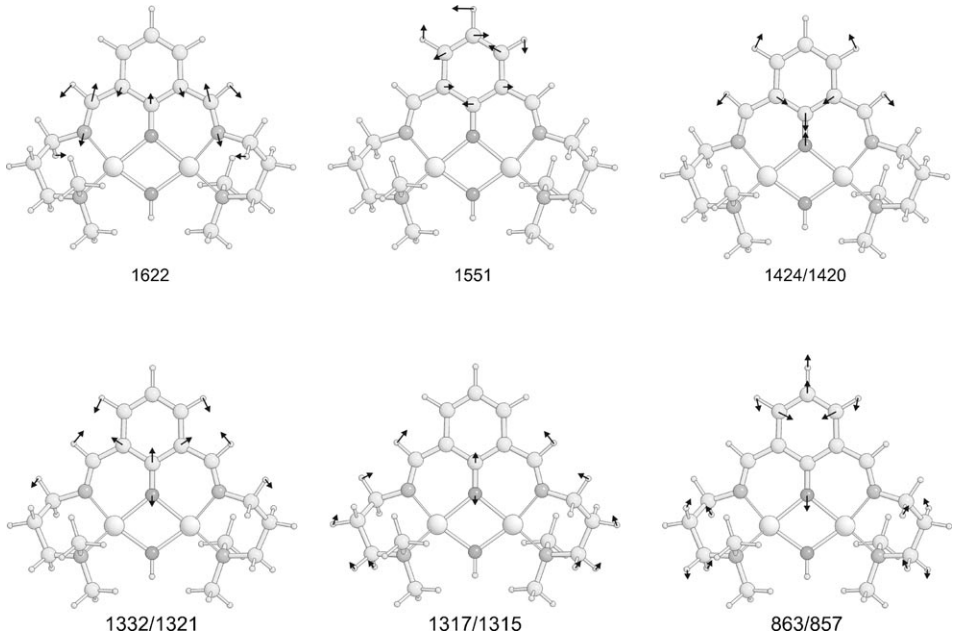

Figure 8. Eigenvectors of the most important vibrations of structure **3** (corresponding to complex **II**).

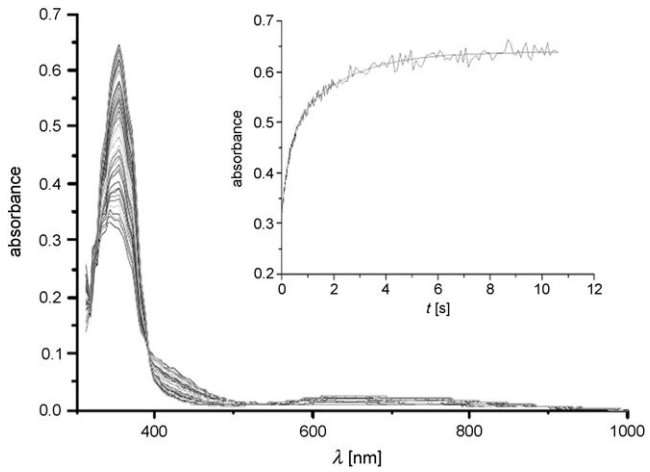

Figure 9. Spectral changes during reaction of **I** with dioxygen in methanol ($T=-60.1\,°C$, [complex] = 0.1 mM, $[O_2]=4.25$ mM, $t=10.605$ s). Inset: Absorbance versus time trace at 353 nm and fit to the sum of two exponentials ($k^1_{obs}=(3.1\pm0.2)$, $k^2_{obs}=(0.41\pm0.03)\ s^{-1}$.

peratures.[15,16] The lack of a detectable O_2 intermediate most likely is the consequence of rate-determining formation of the reactive intermediate and much faster consecutive reactions according to the general Equation (2).

$$[Cu_2L]^{2+} + O_2 \underset{slow}{\xrightarrow{k_1}} [Cu_2L(O_2)] \underset{fast}{\xrightarrow{k_2}} product \qquad (2)$$

Immediately after the dioxygen adduct is formed it further reacts to give the product(s) and therefore cannot be observed spectroscopically. As a consequence, no kinetic data for conversion of the peroxo complex to the hydroxylated product complex could be obtained.

The absorbance versus time traces could be fitted by using one exponential or the sum of two or three exponential functions at different temperatures (see Figure 9). Acceptable fitting over a larger temperature range was, however, not possible. Moreover, we observed a linear dependence on dioxygen concentration for two rate constants with an intercept. This result was not surprising insofar as similar difficulties had been encountered for the complexes $[Cu_2(HBPB\text{-}H)(CH_3CN)_2](BF_4)_2$ (here a more detailed discussion on the different possible reaction pathways has been given) and $[Cu_2(mac)(CH_3CN)_2](ClO_4)_2$ (vide supra). From the present findings we can at least state that one part of the rate law should contain the term $k_{obs}[O_2]$, consistent with the occurrence of a dioxygen adduct as an intermediate. The reaction proved to be faster than observed for $[Cu_2(HBPB\text{-}H)(CH_3CN)_2](BF_4)_2$ and for $[Cu_2(mac)(CH_3CN)_2](ClO_4)_2$ and therefore required low-temperature stopped-flow techniques. This is understandable, as the ligands HBPB-H and mac stabilize the copper(I) complexes better than DAPA.

Hydroxylation of **Ib** leading to **II** was also investigated in acetonitrile. In this case, however, a much slower reaction was observed. This can be attributed to the fact that acetonitrile binds fairly strongly to the Cu^I centers of **Ib** and must be replaced by O_2 in the course of the hydroxylation reaction. Loss of acetonitrile ligands bound to **I** is, of course, impeded if the reaction is performed in this solvent. If, in contrast, the reaction is performed in methanol, the acetonitrile ligands of **Ia** obviously are exchanged in a first reaction step, that is, prior to binding of O_2. This follows from the observation that in this solvent no isotope effect on the binding of O_2 is observed (see below).

In the course of the present study, DFT calculations indicated several thermally accessible pathways from a μ-η^2:η^2 peroxo adduct to the hydroxylated final product (see below) involving proton-transfer steps that should show prominent primary kinetic isotopic effects on ligand deuteration. In order to experimentally check these predictions, further kinetic investigations based on deuterated DAPA complex $\mathbf{I^D}$ were performed. Replacement of **Ib** by $\mathbf{I^D}$ was expected to decrease the reaction rate in the presence of rate-determining H-atom or proton-transfer steps or leave it unchanged in the absence of such reactions.[55] Importantly, the rate of the oxygenation reaction of **Ia** in methanol was unchanged, that is, no significant KIE is present (Figure 10). In acetonitrile, on the other hand, the reaction of $\mathbf{I^D}$ was found to be ap-

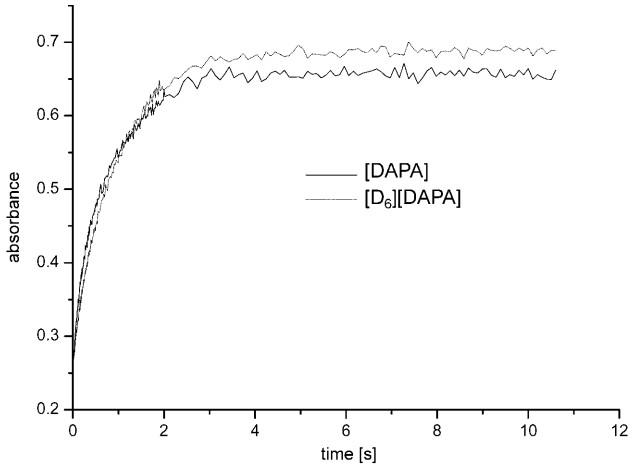

Figure 10. Absorbance during oxygenation of **Ia** at 353 nm in methanol. $T = -60.1\,°C$; [DAPA] = 0.1 mM; [[D_6]DAPA] = 0.1 mM; [O_2] = 4.25 mM; $t = 10.6$ s.

proximately 2.6 times faster (KIE = 0.38) than of **Ib** (Figure 11).

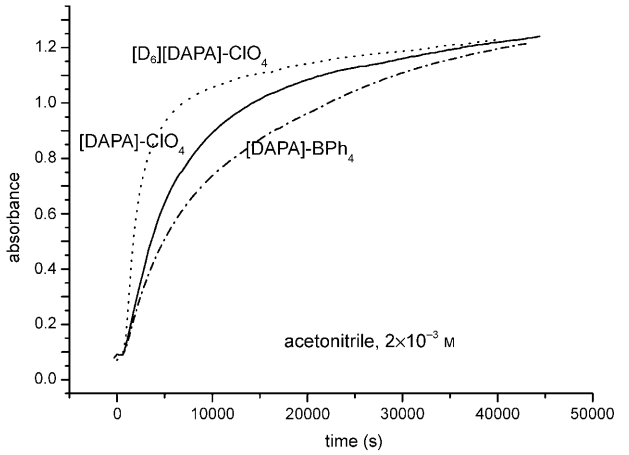

Figure 11. Absorbance at 358 nm for **Ib** (solid), $\mathbf{1^D}$ (dotted), and **Ic** (dash-dotted) during oxygenation in acetonitrile.

The lack of a primary KIE in MeOH and the observation of an inverse deuterium effect in CH_3CN are not compatible with the presence of a rate-determining proton-transfer step in the reaction phase after formation of the σ complex. The inverse deuterium effect in CH_3CN is rather attributed to the reaction phase before formation of the σ complex, that is, binding of O_2: Due to the geometry of the complex the O–O axis in the peroxo adduct points toward the C–H bond of the aromatic ring; O_2 binding thus is hindered by the C–H stretching motion of the H atom at C2 of the phenylene spacer, and due to the smaller C–D vibrational amplitude O_2 binding proceeds faster in the deuterated than in the nondeuterated complex. Since O_2 binding is also the rate-limiting process in methanol, the inverse deuterium effect should in principle appear in this solvent as well. However, this is not observed, and this can be attributed to the fact that this solvent coordinates more weakly than acetonitrile, thus the steric congestion in the transition state leading to the dioxygen adduct is diminished, as is accordingly the influence of the C–H stretching motion on formation of this adduct.

Quantum chemical investigations of reaction pathways: As discussed in the Computational Methods section above, we assume throughout this study that all elementary steps involved in the reaction pathways investigated take place on a ground-state singlet potential-energy surface. In other words, we inherently suppose that the spin flip that evidently occurs on binding of O_2 in its triplet ground state to the bare copper(I) complex occurs as part of the initial steps leading to formation of peroxo complex **1**. These steps, which include solvent exchange at the Cu^I sites and potentially prominent spin-flip phenomena, are not studied here.[56] Instead we concentrate on the fate of the initially formed peroxo Cu_2O_2 species **1** and the elementary steps that are involved in reaction pathways leading to the product of the aromatic hydroxylation (**3**), which corresponds to complex **II**. All relevant intermediates and transition structures are compiled in Figure 12; corresponding energies are collected in Table S1 of the Supporting Information.

Several minima resulted from geometry optimizations performed for the starting point of our quantum chemical investigation, the side-on μ-η^2:η^2-peroxo intermediate **1**; for the sake of brevity we only consider the most stable isomers directly involved in the reaction pathways discussed below. Intermediate **1** exhibits significant butterfly distortion of the Cu_2O_2 moiety, indicative of substantial strain introduced by the ligand framework, which obviously does not allow for the formation of the planar arrangement of this subunit identified experimentally in unstrained systems.[57] Interestingly, we were unable to localize a bis(μ-oxo) isomer for the present ligand environment, although such a species should generally be more stable than the peroxo intermediate for bidentate N-donor ligand environments of Cu_2O_2 cores such as that present here.[8,58] Even carefully preoptimized bis(μ-oxo) structures obtained by constrained-geometry optimizations in which the ideal core substructure was kept fixed while the rest of the structure was optimized fell back into a peroxo structure in subsequent unconstrained optimization runs. We take this finding as another consequence of the significant strain introduced by the ligand framework, which is not flexible enough to allow for the formation of a tighter bis(μ-oxo) core with its closer Cu–Cu contact (2.74–2.79 Å) compared to the larger Cu–Cu distance found in the peroxo cores (3.37–3.56 Å).[57]

Starting from **1** we localized a transition structure (**TS1**) for O–O bond cleavage that resembles to a large extent the corresponding transition structure for the peroxo/bis(μ-oxo) core isomerization identified in our previous study on the aliphatic hydroxylation reactivity of a Cu_2O_2 complex bearing unstrained bidentate N-donor ligands.[59] In the present system, however, **TS1** is a multicenter transition state for si-

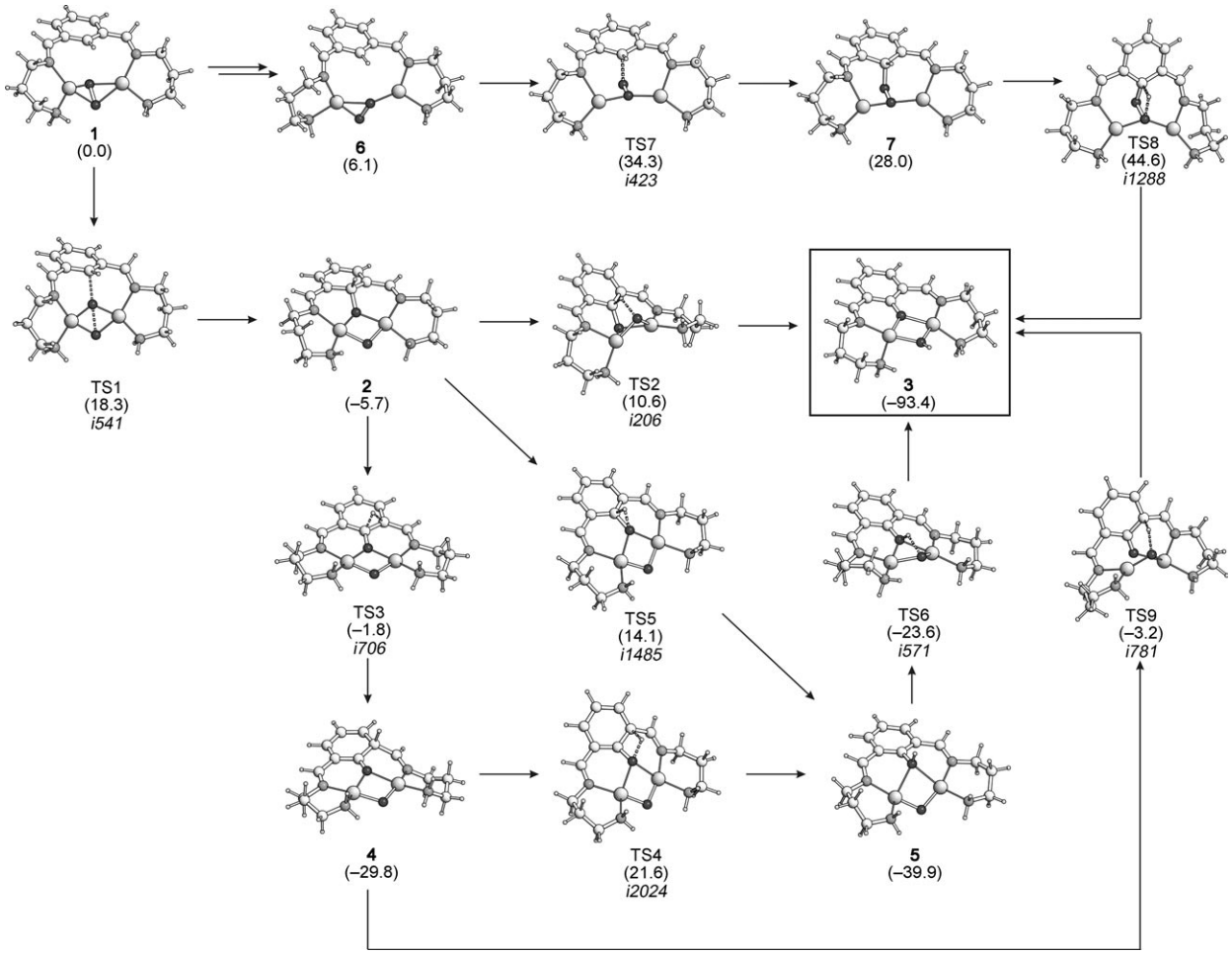

Figure 12. Reaction pathways identified for the hydroxylation reaction starting from μ-η^2:η^2 peroxo complex **1** (Gibbs free energies at 298 K in kcal mol^{-1} relative to **1**; UB3LYP/TZVP + COSMO//UB3LYP/SVP + COSMO results).

multaneous O–O bond cleavage and C–O bond formation. IRC calculations confirm direct connection of this transition state with peroxo minimum **1** and arenium-like σ complex **2**, without occurrence of an intermediate bis(μ-oxo) species. This electrophilic attack of the aromatic ring is connected with a barrier of 18.3 kcal mol^{-1}, and formation of σ intermediate **2** is exoergic by 5.7 kcal mol^{-1}.

We identified three pathways for decay of σ complex **2**. A somewhat unexpected but conceptually strikingly simple path is direct, highly exoergic formation of the final product of the overall reaction, that is, formation of μ-hydroxo μ-phenolato complex **3** ($\Delta G_R = -93.4$ kcal mol^{-1} with respect to **1**) is possible in a single step after passage of **TS2**. In this transition structure the proton at the tetrahedral phenyl carbon atom of σ complex **2** is abstracted by the μ-oxo atom bridging the two copper ions. The unusually low imaginary frequency of *i*206 cm^{-1} for this proton transfer step is a consequence of the participation of several atoms in the transition normal mode resulting from the excessive deformation about the Cu_2O_2 moiety necessary to bend the μ-oxo atom over into bonding range with the transferred proton. Somewhat counterintuitively, however, a rather modest barrier of 16.3 kcal mol^{-1} results for this step, in spite of the highly strained nature of this transition state. Clearly this elementary step profits from significant stabilizing Coulomb interactions between the transferred proton and the high negative charge of the μ-oxo atom (formally O^{2-}). Also, using qualitative Hammond arguments, the large exothermicity of this step ($\Delta G_R = -87.7$ kcal mol^{-1} with respect to **2**) might be seen as another factor contributing to lowering of the barrier. In fact, already at this point product formation appears feasible under the thermal conditions of the experiment: once the barrier of 18.3 kcal mol^{-1} connected with **TS1** is surmounted, subsequent proton transfer via **TS2** should be efficient, as its barrier is even lower, by 2 kcal mol^{-1}.

The situation is, however, more complicated than that. The arenium intermediate **2** can actually rearrange almost without a barrier ($\Delta G^{\neq} = 3.9$ kcal mol^{-1}) via **TS3**, the transition structure of a [1,2] H shift across the phenyl ring, to form the thermodynamically rather stable dienone **4** ($\Delta G_R = -24.1$ kcal mol^{-1}). Hence, any amount of the σ intermediate **2** formed will immediately decay to yield the dienone rather than passing the significantly larger barrier **TS2** that would lead to direct product formation. Decay of the dienone in-

termediate via a [1,3] H shift onto the phenolate oxygen atom to form the more stable phenol intermediate **5** ($\Delta G_R = -10.1$ kcal mol^{-1}) is unlikely to occur because of the excessively high barrier connected with this step via **TS4** ($\Delta G^{\neq} = 51.4$ kcal mol^{-1}). Yet another route to phenol formation was found via **TS5**, which connects σ complex **2** with **5**, but this path has a much higher barrier ($\Delta G^{\neq} = 19.8$ kcal mol^{-1}) than **TS2** and is the kinetically least favorable step among the three routes identified for the decay of **2**. Thus, even though formation of intermediate **5** would provide a strong thermodynamic driving force and subsequent formation of the product complex **3** via **TS6** could occur with a moderately low barrier of 16.3 kcal mol^{-1}, this intermediate is unlikely to play any role in the course of the overall reaction, because unfavorably high barriers preclude its formation from **2**.

With the somewhat unexpected nature of **TS2** in mind we actually located a corresponding transition structure **TS9** leading directly from **4** to the final product **3**, which obviously profits from the same driving force provided by the large proton affinity of the bridging μ-oxo atom. This step is the most favorable pathway we could find for product formation from dienone **4**, and its barrier of 26.6 kcal mol^{-1} appears high enough to prevent an immediate decay of the dienone intermediate. Because all other barriers surrounding **4** are even higher (i.e., reaction back to **2** via **TS3** with $\Delta G^{\neq} = 28.0$ kcal mol^{-1}, or phenol formation via **TS4** with $\Delta G^{\neq} = 51.4$ kcal mol^{-1}), the dienone should be thermodynamically and kinetically stable enough to have a significant lifetime under the experimental conditions. Because the barriers in question are related to proton-transfer transition states, these elementary steps should be subject to substantial KIEs upon deuteration of the 2-position of the phenyl ring. Indeed, H/D exchange of the respective hydrogen atom in the optimized stationary points **4** and **TS9** yields an increase of the corresponding barrier by 1.8 kcal mol^{-1} for the most favorable route for dienone decay. This corresponds to a classical KIE of 21.4 at 298.15 K. Qualitative consideration of quantum mechanical tunneling[60] by employing a simple one-dimensional model[61] significantly increases the predicted KIE to 27.1 (298.15 K). We thus predict a situation in which it may actually be possible to identify this species by experimental means even at room temperature by employing a deuterated ligand framework. Given the fact that it is the only relevant nonaromatic intermediate in the mechanistic scenario established so far, we suggest NMR spectroscopy as a promising tool for its experimental identification.

As an alternative to the reaction paths considered above, we identified a route to product formation commencing with initial rearrangement of the μ-η^2:η^2 peroxo species **1** to μ-η^2:η^1 coordinated isomer **6**, which is less stable than **1** by 6.1 kcal mol^{-1}. From **6** electrophilic attack of the aromatic ring via **TS7** leads to formation of σ complex **7**, a thermodynamically highly unfavorable counterpart of **2** (less stable by 33.7 kcal mol^{-1}). From **7**, proton transfer with simultaneous O–O bond cleavage via **TS8** leads to formation of hydroxylated product **3**. With formation of two thermodynamically unfavorable intermediates and two energetically demanding reaction barriers, this reaction sequence can effectively be seen as a unimolecular decomposition of **1** (assuming reaction kinetics with pre-equilibrium) with an overall barrier of 44.6 kcal mol^{-1} related to **TS8**. Thus, with the highest effective barrier identified in our entire study, this reaction channel is unlikely to contribute to product formation.

In summary, we identified four alternative reaction pathways leading from μ-η^2:η^2 peroxo species **1** to hydroxylated product **3**. The three thermally accessible pathways all involve decay of σ intermediate **2**. Formation of **2** requires passing an activation barrier of 18.3 kcal mol^{-1} via **TS1** corresponding to electrophilic attack on the aromatic ring by the peroxo Cu_2O_2 core. Intermediate **2** can rearrange almost without activation barrier to dienone intermediate **4**, which we propose as a key intermediate in the course of the aromatic hydroxylation reaction. For the energetically least demanding route leading from **4** to product formation via **TS9** we predict an effective barrier of 26.6 kcal mol^{-1}. Consequently, for the overall mechanistic scenario established here, this last proton transfer is the rate-limiting step for product formation. The preceding electrophilic attack via **TS1** is energetically significantly less demanding, by 8.3 kcal mol^{-1}. For the rate-limiting step we predict a large H/D KIE, which may allow future characterization of the dienone intermediate by NMR techniques.

Why then did the dienone intermediate escape any experimental detection in our hands so far? An intuitively striking explanation for the experiments performed in methanol is participation of this protic solvent in the proton-transfer steps in the latter phase of the reaction sequence. In this case intermolecular proton transfer steps will most likely provide much lower barriers than those identified in our computations, which were performed with a continuum solvent model but without explicit consideration of solvent molecules. But also in experiments in aprotic solvents, we searched in vain for any trace of this intermediate. Spurred by recent reports on the potential importance of counterions for related systems[53,62] we investigated the influence of a single ClO_4^- counterion on the rate-limiting step of the mechanistic scenario suggested above. Indeed, compared to the computed barrier height of 26.6 kcal mol^{-1} for the step **4**→**TS9** a dramatically lower barrier of only 7.5 kcal mol^{-1} results for the corresponding process **4**·ClO_4→**TS9**·ClO_4 (Figure 13). This result implies a high reaction rate for this elementary step at room temperature, which straightforwardly explains the lack of any experimental evidence for the occurrence of a stable dienone intermediate prior to product formation or any prominent KIE in acetonitrile or CH_2Cl_2.

To substantiate this quantum chemical result the hydroxylation reaction was repeated in the aprotic solvent acetonitrile, with the Cu^I DAPA complex in the form of its salt with the noncoordinating anion BPh_4 (**Ic**). Under these conditions a significantly slower reaction than with perchlorate as counterion (**Ib**) was observed (see Figure 11). This

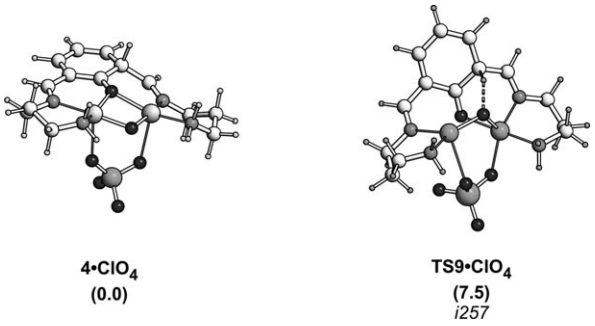

Figure 13. Dienone **4**·ClO_4 and transition structure **TS9**·ClO_4 leading to product formation optimized in the presence of a coordinating ClO_4^- counterion (Gibbs free energies at 298 K in kcal mol^{-1} relative to **4**·ClO_4; UB3LYP/TZVP + COSMO//UB3LYP/SVP + COSMO results).

indeed supports the presence of a rate-limiting proton-transfer step leading from the dienone to the final product, which is markedly accelerated in the presence of a coordinating counterion.

Discussion and Conclusion

Structural, spectroscopic, kinetic, and quantum chemical investigations of the ligand hydroxylation reaction mediated by a Cu bis(imine) complex have been presented. Starting from a structural analysis of the Cu^I complex **I** and the Cu^{II} product **II** exhibiting a hydroxylated ligand the optical absorption and vibrational spectra were analyzed. Special attention was directed to reproducing the structural and spectroscopic properties of complex **II** by quantum chemical means. Kinetic analysis of ligand hydroxylation provided evidence for O_2 binding as the rate-limiting step in the overall reaction. Conversion of **I** to **II** was found to proceed much faster in methanol than in acetonitrile, which was attributed to the fact that the acetonitrile ligands of the Cu^I precursor **I** are displaced in the course of O_2 binding. Moreover, an inverse KIE was evidenced for the reaction in acetonitrile, which was rationalized by a sterically congested transition state leading to the peroxo adduct. In methanol, however, no KIE was observed. Finally, a DFT analysis of the oxygenation reaction demonstrated that the dominant barrier after O_2 binding is represented by electrophilic attack of μ-η^2:η^2 peroxo intermediate **1** on the arene ring. Nevertheless, on the basis of the activation energy (18.3 kcal mol^{-1}) this reaction is thermally allowed, in agreement with the experimental observation. Given that the B3LYP functional employed has been shown to overestimate barrier heights by 4–7 kcal mol^{-1},[63] the actual barrier height may be in the range of 10–15 kcal mol^{-1}.

The DFT investigation of the reactivity of the Cu^{II} peroxo intermediate **1** formed by reaction of the Cu^I precursor and O_2 indicated the presence of four pathways to the hydroxylated final product **3**. One of the pathways studied involves rearrangement of the μ-η^2:η^2 peroxo structure to a μ-η^2:η^1 peroxo intermediate that subsequently attacks the aromatic ring. In the present system, however, this pathway is associated with an overall barrier of 44.6 kcal mol^{-1}, which renders it less likely for product formation. In this context it is interesting to note that Siegbahn has suggested a related sequence (i.e., peroxide attack followed by O–O bond cleavage) as key steps for the *ortho*-hydroxylation of phenolate in the catalytic cycle of tyrosinase, but with an overall barrier of only 14.4 kcal mol^{-1}.[13] Alternative pathways were not reported in this study. In contrast, all energetically favorable pathways identified in our study involve direct decay of the μ-η^2:η^2 peroxo intermediate **1** without rearrangement to an alternative peroxide coordination mode.

The energetically most favorable route commences with direct electrophilic attack of the aromatic ring by the peroxo moiety to form an arenium ion, which subsequently undergoes an almost barrierless proton shift to form a rather stable dienone intermediate (**4**). A second proton-transfer step from the dienone directly leads to product formation. We have identified several alternative pathways with moderate barrier heights that would actually be thermally accessible under the experimental conditions. None of these pathways, however, can compete with the energetically most favorable pathway, even assuming potential errors in computed relative energies as large as 7 kcal mol^{-1}, and so we feel safe in suggesting a single pathway as a general mechanistic scenario for the system under study.

This scenario involves as a key intermediate in the conversion of the peroxo complex to the hydroxylated product the dienone intermediate **4**, which should eventually be detectable experimentally. We attribute the fact that we (and others) were unable so far to identify such an intermediate to several factors: first, explicit participation of protic (or Lewis basic) solvent molecules (which have not been considered in our calculations) in the proton transfer steps after formation of σ complex **2** may lead to drastically lowered barriers. Second, the key proton-transfer steps may occur in an intermolecular fashion, involving initial deprotonation of the σ complex by another copper dioxygen intermediate. A third factor contributing to the rapid decay of the dienone the counterion was explicitly identified in the computations: Compared to the calculated barrier height of 26.6 kcal mol^{-1} for the decay of **4** via **TS9**, a dramatically lowered barrier of 7.5 kcal mol^{-1} was found for the corresponding process **4**·ClO_4→**TS9**·ClO_4→product (**3**). This hypothesis is supported by kinetic measurements on the BPh_4^- salt of the Cu^I_2 DAPA complex (**Ic**), for which a significantly lower reaction rate was found compared to corresponding perchlorate salt **Ib**. To directly detect dienone intermediate **4** further experimental studies must be performed. The present system, however, appears less suitable for these investigations, as binding of O_2 is also associated with a thermal barrier which probably precludes accumulation of a dienone species at low temperatures.

Another notable and somewhat surprising result of our quantum chemical analysis is the finding that no stable bis-(μ-oxo) isomer is formed in the ligand environment studied

here. Based on the experience gathered in related investigations by others, we would actually expect preferential formation of a bis(μ-oxo) species within the chelating bidentate N-donor ligand environment of the system studied here. Yet, the initial steps take place without intermediate formation of a bis(μ-oxo) species. While the initial transition state **TS1** exhibits structural features nearly identical to O–O bond-breaking transition states leading to the formation of a bis(μ-oxo) species in related ligand environments,[59] in the present case it is a multicenter transition state for O–O bond cleavage and simultaneous σ attack of the aromatic ring by the peroxo moiety. We view this finding as a consequence of the rather tight coordination sphere of the bis(imine) ligand, which brings the breaking O–O bond in the Cu_2O_2 subunit in **TS1** into close proximity to the aromatic ring, ideally oriented for direct orbital interactions with the aromatic π system to generate σ complex **2** in a single step.

The mechanistic scenario established here has implications for the ligand hydroxylation reaction occurring in the prototype binuclear copper complex [Cu_2(XYL)] of Karlin et al.[15] on reaction with O_2. In full agreement with our present results, Pidcock et al. implied a μ-η^2:η^2 peroxo complex as active species and excluded the occurrence of a corresponding bis(μ-oxo) species in a spectroscopic analysis of this reaction.[16] They rationalized the electrophilic attack of the Cu_2O_2 moiety on the aromatic ring in terms of qualitative frontier orbital arguments. Within this picture, it was convincingly argued that the HOMO of the arene system overlaps with an unoccupied orbital of the electrophile, which can either be the π_σ^* or the σ* orbital of the side-on peroxo dicopper core (Figure 14a). Based on the particularities of the coordination geometry present in the tridendate ligand environment in that study, an attack via the σ* peroxide orbital was considered unlikely, and a preferred, symmetry allowed pathway involving the π_σ^* orbital was suggested. The geometry of the initial transition state **TS1** optimized for the copper bis(imine) complex here, however, differs essentially from the assumed transition state geometry discussed by Pidcock et al., and it is in fact the σ* orbital of the peroxo group, and not the π_σ^* orbital, that is involved in the electrophilic attack on the arene ring. In particular, the rather rigid ligand framework studied in the present work does not allow tilting of the aromatic ring along the O–O axis of the Cu_2O_2 group in the course of this elementary step, which would indeed exclude any constructive orbital interaction between the σ* peroxo orbital and the aromatic π system. Instead the arene ring and the Cu_2O_2 group rotate in the transition state about axes perpendicular to the O–O vector such that the σ* orbital now interacts with the aromatic π system from below in a symmetry-allowed fashion that mediates the initial step along the hydroxylation pathway (Figure 14b).

Another interesting implication for the mechanism of the XYL system relates to the observation of an NIH shift in studies employing a modified xylyl ligand that was methylated at the 2-position of the aromatic core.[64] This observation could in fact straightforwardly be rationalized by assuming

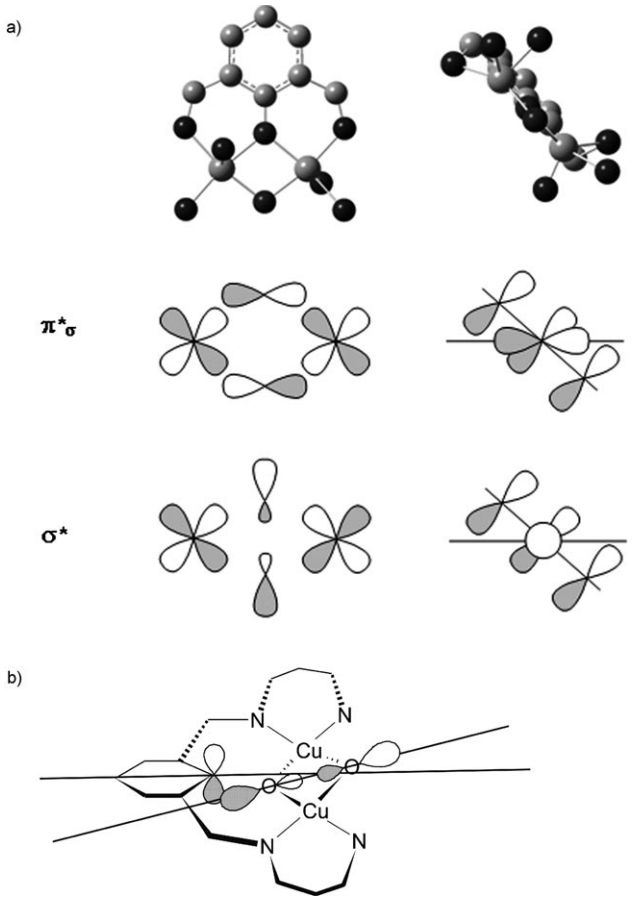

Figure 14. Geometries in the transition states leading to the σ complex. a) Complex of Karlin et al. b) Bis(imine) complex (see text).[16]

formation of a dienone as a key intermediate, in analogy to the mechanistic scenario developed here. A subsequent C–N cleavage, in analogy to the cleavage of the methylene–N(amine) bond in the XYL system, would, however, appear unlikely in a bis(imine) complex due to the double-bond character of the C–N linkage.

The present results are also relevant to the enzyme tyrosinase, specifically the *ortho*-hydroxylation of tyrosine mediated by the oxy form of this enzyme. Of crucial importance for this reaction is the orientation of phenolic substrates with respect to the binuclear copper active site. Experimental information on this point has mostly been derived from spectroscopic studies on the bonding of inhibitors to tyrosinase.[65] Alternatively, it has been proposed that an external tyrosine substrate is oriented at the active site of Ty in the same way as Phe49 in the *Limulus oxy* Hc structure.[66] The recently solved structure of *Streptomyces castaneoglobisporus* tyrosinase revealed a very similar arrangement with Tyr98 (provided by the associated caddie protein) extending into the active-site pocket like a potential substrate.[1,2] An external phenolic substrate may be preoriented at the active site in a similar geometry (Scheme 2). Then a slight shift towards CuA is necessary to bind in the position *trans* to His63, after which hydroxylation of the aromatic ring can

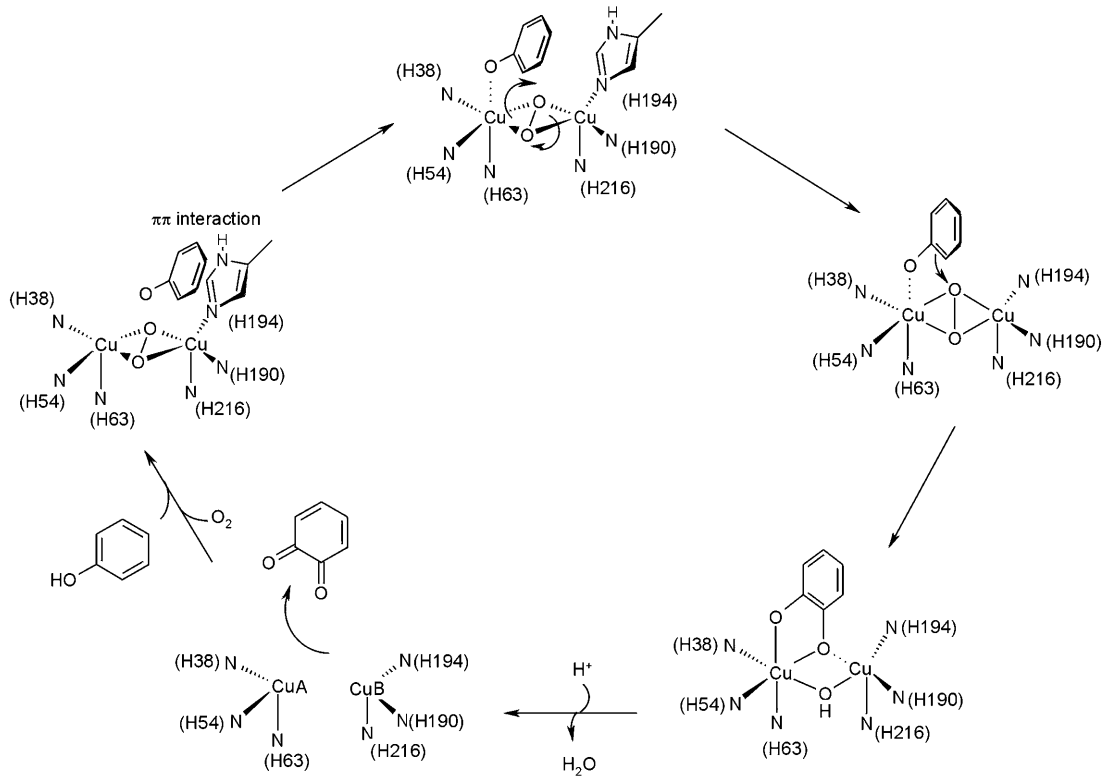

Scheme 2. Hydroxylation/oxidation of monophenolic substrates in tyrosinase from *Streptomyces castaneoglobisporus* (adapted from ref. [2], see text).

occur. Importantly, the proximity of the *ortho* position of the phenolic ring to the side-on-coordinated peroxo group enables electrophilic attack of the Cu_2O_2 moiety on the aromatic ring.[2,16] To this end, the O–O axis of the peroxo ligand may rotate to point towards the substrate (Scheme 2). This geometry would correspond to the transition state **TS1** in our complex leading to σ complex **2** and would involve an orbital interaction between the peroxide σ* orbital and the HOMO of the aromatic ring, in analogy to our model system.

The analysis of the hydroxylation pathway in the Cu_2 bis(imine) complex thus has shown that besides the previously discussed π_σ^* pathway a second pathway for the oxygenation chemistry mediated by binuclear copper site does exist, that is, electrophilic attack on the substrate by the σ* orbital of side-on bound peroxide. For systems exhibiting more structural flexibility than the Cu bis(imine) systems, both pathways may be operative. Importantly, the presence of a second orbital pathway provides additional flexibility for the position of the aromatic substrate with respect to the Cu_2O_2 unit in the transition state leading to the σ complex. This is of relevance both for the enzyme tyrosinase and for copper model systems which are active in the hydroxylation of external substrates.[67] In all of these cases the σ* orbital directed along the prolonged O–O vector just has to "hit" the π system of the substrate (except for the nodal plane of the C orbitals) from an arbitrary angle to mediate hydroxylation. This structural flexibility in the transition state accounts for the wide occurrence of oxygenation reactions in binuclear copper–dioxygen systems exhibiting widely different ligand structures and explains why these reactions are not limited to a few systems with special geometries.

Acknowledgement

F.T. thanks CAU Kiel and COST D21 for financial support and F. Studt for preliminary calculations. O.S. acknowledges help of U. Cornelissen with the Raman and IR measurements. Computer time provided by the CSC Frankfurt, the HHLR Darmstadt, and the HRZ Marburg is gratefully acknowledged.

[1] Y. Matoba, T. Kumagai, A. Yamamoto, H. Yoshitsu, M. Sugiyama, *J. Biol. Chem.* **2006**, *281*, 8981.
[2] H. Decker, T. Schweikhardt, F. Tuczek, *Angew. Chem.* **2006**, *118*, 4658; *Angew. Chem. Int. Ed.* **2006**, *45*, 4546.
[3] E. I. Solomon, U. M. Sundaram, T. E. Machonkin, *Chem. Rev.* **1996**, *96*, 2563.
[4] A. Sanchez-Ferrer, J. N. Rodríguez-López, F. García-Cánovas, F. García-Carmona, *Biochim. Biophys. Acta* **1995**, *210*, 1.
[5] C. Eicken, C. Gerdemann, B. Krebs, *Handbook of Metalloproteins, Vol. 2* (Eds.: A. Messerschmidt, R. Huber, T. Poulos, K. Wieghardt), Wiley, New York, **2001**, pp. 1319.
[6] M, Trèmolières, J. B. Bieth, *Phytochem.* **1984**, *23*, 501.
[7] a) K. E. van Holde, K. I. Miller, H. Decker, *J. Biol. Chem.* **2001**, *276*, 15563; b) H. Decker in *Encyclopedia of Inorganic Chemistry, Vol. 2*, 2nd ed. (Ed.: R. B. King), Wiley, New York, **2006**, pp. 1159–1173.
[8] E. A. Lewis, W. B. Tolman, *Chem. Rev.* **2004**, *104*, 1047.
[9] L. Li, A. N. Sarjeant, K. D. Karlin, *Inorg. Chem.* **2006**, *45*, 7160.

[10] D. Ghosh, R. Mukherjee, *Inorg. Chem.* **1998**, *37*, 6597.
[11] S. B. Foxon, D. Utz, J. Astner, S. Schindler, F. Thaler, F. W. Heinemann, G. Liehr, J. Mukherjee, V. Balamurugan, D. Ghosh, R. Mukherjee, *Dalton Trans.* **2004**, 2321
[12] P. E. M. Siegbahn, M. Wirstam, *J. Am. Chem. Soc.* **2001**, *123*, 11819.
[13] P. E. M. Siegbahn, *J. Biol. Inorg. Chem.* **2003**, *8*, 567.
[14] S. Itoh, M. Taki, H. Nakao, P. L. Holland, W. B. Tolman, L. Que, Jr., S. Fukuzumi, *Angew. Chem.* **2000**, *112*, 409; *Angew. Chem. Int. Ed.* **2000**, *39*, 398.
[15] a) K. D. Karlin, P. L. Dahlstrom, S. N. Cozzette, P. M. Scensny, J. Zubieta, *J. Chem. Soc. Chem. Commun.* **1981**, 881; b) K. D. Karlin, J. C. Hayes, Y. Gultneh, R. W. Cruse, J. W. McKown, J. P. Hultchinson, J. Zubieta, *J. Am. Chem. Soc.* **1984**, *106*, 2121–2128.
[16] E. Pidcock, H. V. Obias, C. X. Zhang, K. D. Karlin, E. I. Solomon, *J. Am. Chem. Soc.* **1998**, *120*, 7841.
[17] a) L. M. Mirica, M. Vance, D. Jackson Rudd, B. Hedman, K. O. Hodgson, E. I. Solomon, T. D. P. Stack, *Science* **2005**, *308*, 1890; b) L. M. Mirica, D. J. Rudd, M. A. Vance, E. I. Solomon, K. O. Hodgson, B. Hedman, T. D. P. Stack, *J. Am. Chem. Soc.* **2006**, *128*, 2654; c) A. Company, S. Palavicini, I. Garcia-Bosch, R. Mas-Ballesté, L. Que, Jr., E. Rybak-Akimova, L. Casella, X. Ribas, M. Costas, *Chem. Eur. J.* **2008**, *14*, 3535.
[18] P. L. Holland, K. R. Rodgers, W. B. Tolman, *Angew. Chem.* **1999**, *111*, 1210; *Angew. Chem. Int. Ed.* **1999**, *38*, 1139.
[19] B. L. Feringa in *Bioinorganic Chemistry of Copper* (Eds.: K. Karlin, Z. Tyeklár), Chapman and Hall, New York, **1993**, pp. 306–324.
[20] P. Amudha, P. Akilan, M. Kandaswamy, *Polyhedron* **1999**, *18*, 1355.
[21] D. Utz, F. W. Heinemann, F. Hampel, D. T. Richens, S. Schindler, *Inorg. Chem.* **2003**, *42*, 1430.
[22] L. Casella, M. Gullotti, G. Pallanza, L. Rigoni, *J. Am. Chem. Soc.* **1988**, *110*, 4221.
[23] S. Ryan, H. Adams, D. E. Fenton, M. Becker, S. Schindler, *Inorg. Chem.* **1998**, *37*, 2134–2140.
[24] R. Menif, A. E. Martell, P. J. Squattrito, A. Clearfield, *Inorg. Chem.* **1990**, *29*, 4723–4729.
[25] G. J. Kubas, B. Monzyk, A. L. Crumbliss, *Inorg. Synth.* **1979**, *19*, 90.
[26] S. V. Kryatov, E. V. Rybak-Akimova, S. Schindler, *Chem. Rev.* **2005**, *105*, 2175.
[27] M. Weitzer, M. Schatz, F. Hampel, F. W. Heinemann, S. Schindler, *Dalton Trans.* **2002**, 686.
[28] M. G. B. Drew, J. Trocha-Grimshaw, K. P. McKillop, *Polyhedron* **1989**, *8*, 2513.
[29] The B3LYP/G functional corresponds to that implemented in the Gaussian 03 program: a) A. D. Becke, *J. Chem. Phys.* **1993**, *98*, 5648; b) A. D. Becke, *Phys. Rev. A* **1988**, *38*, 3098; c) C. Lee, W. Yang, R. G. Parr, *Phys. Rev. B* **1988**, *37*, 785; d) P. J. Stephens, F. J. Devlin, C. F. Chabalowski, M. J. Frisch, *J. Phys. Chem.* **1994**, *98*, 11623.
[30] F. Neese, ORCA—An ab initio, DFT and semiempirical SCF-MO package, Version 2. 5. 00, Universität Bonn, Germany, **2006**.
[31] A. Schaefer, H. Horn, R. Ahlrichs, *J. Chem. Phys.* **1992**, *97*, 2571.
[32] a) F. Neese, *J. Comput. Chem.* **2003**, *24*, 1740; b) F. Neese, G. Olbrich, *Chem. Phys. Lett.* **2002**, *362*, 170.
[33] a) K. Eichkorn, O. Treutler, H. Ohm, M. Häser, R. Ahlrichs, *Chem. Phys. Lett.* **1995**, *240*, 283; b) K. Eichkorn, F. Weigend, O. Treutler, R. Ahlrichs, *Theor. Chem. Acc.* **1997**, *97*, 119.
[34] R. A. Kendall, H. A. Früchtl, *Theor. Chem. Acc.* **1997**, *97*, 158.
[35] a) A. Klamt, G. Schürmann, *J. Chem. Soc. Perkin Trans. 2* **1993**, 799; b) A. Klamt in *Encylopedia of Computational Chemistry* (Eds.: N. L. Allinger, T. Clark, J. Gasteiger, P. Kollmann, H. F. Schaefer III, P. von R. Schleyer, P. R. Schreiner), Wiley, Chichester, **1998**, p. 604.
[36] We successfully repeated some of the transition-state searches with identical results (to numerical accuracy) with the extended geometry optimization routines implemented in the most recent ORCA Version 2.6.35, which was made available to us by the Bonn developer group after this project was about to be finished.
[37] Gaussian 03, Revision B3, M. J. Frisch, G. W. Trucks, H. B. Schlegel, G. E. Scuseria, M. A. Robb, J. R. Cheeseman, J. J. A. Montgomery, T. Vreven, K. N. Kudin, J. C. Burant, J. M. Millam, S. S. Iyengar, J. Tomasi, V. Barone, B. Mennucci, M. Cossi, G. Scalmani, N. Rega, G. A. Petersson, H. Nakatsuji, M. Hada, M. Ehara, K. Toyota, R. Fukuda, J. Hasegawa, M. Ishida, T. Nakajima, Y. Honda, O. Kitao, H. Nakai, M. Klene, X. Li, J. E. Knox, H. P. Hratchian, J. B. Cross, C. Adamo, J. Jaramillo, R. Gomperts, R. E. Stratmann, O. Yazyev, A. J. Austin, R. Cammi, C. Pomelli, J. W. Ochterski, P. Y. Ayala, K. Morokuma, G. A. Voth, P. Salvador, J. J. Dannenberg, V. G. Zakrzewski, S. Dapprich, A. D. Daniels, M. C. Strain, O. Farkas, D. K. Malick, A. D. Rabuck, K. Raghavachari, J. B. Foresman, J. V. Ortiz, Q. Cui, A. G. Baboul, S. Clifford, J. Cioslowski, B. B. Stefanov, G. Liu, A. Liashenko, P. Piskorz, I. Komaromi, R. L. Martin, D. J. Fox, T. Keith, M. A. Al-Laham, C. Y. Peng, A. Nanayakkara, M. Challacombe, P. M. W. Gill, B. Johnson, W. Chen, M. W. Wong, C. Gonzalez, J. A. Pople, Gaussian, Inc, Pittsburgh, PA, **2003**.
[38] L. Noodleman, T. Lovell, W.-G. Han, J. Li, F. Himo, *Chem. Rev.* **2004**, *104*, 459.
[39] a) L. Noodleman, *J. Chem. Phys.* **1981**, *74*, 5737; b) L. Noodleman, E. J. Baerends, *J. Am. Chem. Soc.* **1984**, *106*, 2316; c) L. Noodleman, E. R. Davidson, *Chem. Phys.* **1986**, *109*, 131; d) L. Noodleman, D. A. Case, *Adv. Inorg. Chem.* **1992**, *38*, 423; e) L. Noodleman, J. Li, X. -G. Zhao, W. H. Richardson in *Density-functional Methods in Chemistry and Materials* (Ed.: M. Springborg), Wiley, New York, **1997**.
[40] a) K. Yamaguchi, Y. Takahara, T. Fueno in *Applied Quantum Chemistry* (Eds.: V. H. Smith, Jr., H. F. Schaefer III, K. Morokuma), Reidel, Dordrecht, **1986**, p. 155. b) T. Soda, Y. Kitagawa, T. Onishi, Y. Takano, Y. Shigeta, H. Nagao, Y. Yoshioka, K. Yamaguchi, *Chem. Phys. Lett.* **2000**, *319*, 223–230.
[41] F. Neese, *J. Phys. Chem. Solids* **2004**, *65*, 781.
[42] a) T. Saito, Y. Kitagawa, M. Shoji, Y. Nakanishi, M. Ito, T. Kawakami, M. Okumura, K. Yamaguchi, *Chem. Phys. Lett.* **2008**, *456*, 76; b) I. de P. R. Moreira, R. Costa, M. Filatov, F. Illas, *J. Chem. Theory Comput.* **2007**, *3*, 764; c) F. Illas, I. de P. R. Moreira, J. M. Bofill, M. Filatov, *Theor. Chem. Acc.* **2006**, *116*, 587; d) I. Ciofini, C. A. Daul, *Coord. Chem. Rev.* **2003**, *238–239*, 187; e) A. Rodríguez-Fortea, P. Alemany, S. Alvarez, E. Ruiz, *Inorg. Chem.* **2002**, *41*, 3769; f) C. Despanches, E. Ruiz, A. Rodríguez-Fortea, S. Alvarez, *J. Am. Chem. Soc.* **2002**, *124*, 5197; g) J. Cano, E. Ruiz, P. Alemany, F. Lloret, S. Alvarez, *J. Chem. Soc. Dalton Trans.* **1999**, 1669; h) E. Ruiz, J. Cano, S. Alvarez, P. Alemany, *J. Am. Chem. Soc.* **1998**, *120*, 11122; i) F. Bernardi, A. Bottoni, R. Casadio, P. Fariselli, A. Rigo, *Inorg. Chem.* **1996**, *35*, 5207; j) A. Bencini, D. Gatteschi *J. Am. Chem. Soc.* **1986**, *108*, 5763.
[43] M. C. Holthausen *J. Comput. Chem.* **2005**, *26*, 1505.
[44] a) S. Shaik, D. Danovich, A. Fiedler, D. Schröder, H. Schwarz, *Helv. Chim. Acta* **1995**, *78*, 1393; b) D. Schröder, S. Shaik, H. Schwarz, *Acc. Chem. Res.* **2000**, *33*, 139; c) H. Schwarz, *Int. J. Mass Spectrom.* **2004**, *237*, 75.
[45] a) D. Schröder, M. C. Holthausen, H. Schwarz, *J. Phys. Chem. B* **2004**, *108*, 14407; b) J. N. Harvey, *Phys. Chem. Chem. Phys.* **2007**, *9*, 331.
[46] a) A. D. Becke, *Phys. Rev. A* **1988**, *38*, 3098; b) J. B. Perdew, *Phys. Rev. B* **1986**, *33*, 8822.
[47] M. Schatz, V. Raab, S. P. Foxon, G. Brehm, S. Schneider, M. Reiher, M. C. Holthausen, J. Sundermeyer, S. Schindler, *Angew. Chem.* **2004**, *116*, 4460; *Angew. Chem. Int. Ed.* **2004**, *43*, 4360.
[48] Compare Chapter 8 in W. Koch, M. C. Holthausen, *A Chemist's Guide to Density Functional Theory*, 2nd ed., Wiley-VCH, Weinheim, **2001**.
[49] S. Mandal, R. Mukherjee, *Inorg. Chim. Acta* **2006**, *359*, 4019.
[50] O. J. Gelling, F. v. Bolhuis, A. Meetsma, B. L. Feringa, *J. Chem. Soc. Chem. Commun.* **1988**, 552.
[51] K. D. Karlin, Y. Gultneh, J. P. Hutchinson, J. Zubieta, *J. Am. Chem. Soc.* **1982**, *104*, 5240.
[52] H. Ma, M. Allmendinger, U. Thewalt, A. Lentz, M. Klinga, B. Rieger, *Eur. J. Inorg. Chem.* **2002**, *11*, 2857–2867.
[53] A. Company, L. Gomez, R. Mas-Balleste, I. V. Korendovych, X. Rabas, A. Poater, T. Parella, X. Fontodora, J. Benet-Buchholz, M. Sola, L. Que, Jr., E. V. Rybak-Akimova, M. Costas, *Inorg. Chem.* **2007**, *46*, 4997.

[54] J. W. Pyrz, K. D. Karlin, T. N. Sorrell, G. C. Vogel, L. Que, Jr., *Inorg. Chem.* **1984**, *23*, 4581.
[55] S. Mahaptra, J. A. Halfen, W. B. Tolman, *J. Am. Chem. Soc.* **1996**, *118*, 11575.
[56] a) M. Metz, E. I. Solomon, *J. Am. Chem. Soc.* **2001**, *123*, 4938; b) E. I. Solomon, P. Chen, M. Metz, S. -K. Lee, A. E. Palmer, *Angew. Chem.* **2001**, *113*, 4702; *Angew. Chem. Int. Ed.* **2001**, *40*, 4570; c) Y. Takano, K. Yamaguchi, *Int. J. Quant. Chem.* **2007**, *107*, 3103; d) P. Chen, D. E. Root, C. Campochiaro, K. Fujisawa, E. I. Solomon, *J. Am. Chem. Soc.* **2003**, *125*, 466; e) C. J. Cramer, W. B. Tolman, K. H. Theopold, A. L. Rheingold, *Proc. Natl. Acad. Sci. USA* **2003**, *100*, 3635; f) D. A. Pantazis, J. W. McGrady, *Inorg. Chem.* **2003**, *42*, 7734; g) C. J. Cramer, W. B. Tolman, *Acc. Chem. Res.* **2007**, *40*, 601; h) B. F. Gherman, C. J. Cramer, *Inorg. Chem.* **2004**, *43*, 7281.
[57] a) N. Kitajima, K. Fujisawa, Y. Moro-Oka, K. Toriumi, *J. Am. Chem. Soc.* **1989**, *111*, 8975; b) L. Mirica, X. Ottenwaelder, D. T. P. Stack, *Chem. Rev.* **2004**, *104*, 1013.
[58] a) W. B. Tolman, *Acc. Chem. Res.* **1997**, *30*, 227; b) V. Mahadevan, Z. Hou, A. P. Cole, D. E. Root, T. K. Lal, E. I. Solomon, T. D. P. Stack, *J. Am. Chem. Soc.* **1997**,*119* 11996; c) H. V. Obias, Y. Lin, N. N. Murthy, E. Pidcock, E. I. Solomon, M. Ralle, N. J. Blackburn, Y. -M. Neuhold, A. D. Zuberbühler, K. D. Karlin, *J. Am. Chem. Soc.* **1998**, *120*, 12960; d) E. Pidcock, S. DeBeer, H. V. Obias, B. Hedman, K. O. Hodgson, K. D. Karlin, E. I. Solomon, *J. Am. Chem. Soc.* **1999**, *121*, 1870; e) V. Mahadevan, M. J. Henson, E. I. Solomon, T. D. P. Stack, *J. Am. Chem. Soc.* **2000**, *122*, 10249; f) M. Taki, S. Teramae, S. Nagatomo, Y. Tachi, T. Kitagewa, S. Itoh, S. Fukuzumi, *J. Am. Chem. Soc.* **2002**, *124*, 6367; g) M. J. Henson, C. Liang, K. D. Karlin, E. I. Solomon, *J. Am. Chem. Soc.* **2003**, *125*, 5186; h) T. D. P. Stack, *Dalton Trans.* **2003**, 881.
[59] P. Spuhler, M. C. Holthausen, *Angew. Chem.* **2003**, *115*, 6143; *Angew. Chem. Int. Ed.* **2003**, *42*, 5961.
[60] R. Berger, *Angew. Chem.* **2004**, *116*, 402; *Angew. Chem. Int. Ed.* **2004**, *43*, 398.
[61] R. T. Skodje, D. G. Truhlar, *J. Phys. Chem.* **1981**, *85*, 624.
[62] X. Ottenwaelder, D. J. Rudd, M. C. Corbett, K. O. Hodgson, B. Hedman, T. D. P. Stack, *J. Am. Chem. Soc.* **2006**, *128*, 9268.
[63] S. S. Yi, E. L. Reichert, M. C. Holthausen, W. Koch, J. C. Weisshaar, *Chem. Eur. J.* **2000**, *6*, 2232.
[64] a) K. D. Karlin, B. I. Cohen, R. R. Jacobson, J. Zubieta, *J. Am. Chem. Soc.* **1987**, *109*, 6194; b) M. S. Nasir, B. I. Cohen, K. D. Karlin, *J. Am. Chem. Soc.* **1992**, *114*, 2482.
[65] a) R. S. Himmelwright, N. C. Eickman, C. D. LuBien, E. I. Solomon, K. Lerch, *J. Am. Chem. Soc.* **1980**, *102*, 7339; b) A. W. Tepper, L. Bubacco, G. W. Canters, *J. Am. Chem. Soc.* **2005**, *127*, 567.
[66] a) H. Decker, R. Dillinger, F. Tuczek, *Angew. Chem.* **2000**, *112*, 1656; *Angew. Chem. Int. Ed.* **2000**, *39*, 1591; b) H. Decker, F. Tuczek, *Trends Biochem. Sci.* **2000**, *25*, 392.
[67] a) L. Casella, M. Gulotti, R. Radaelli, P. Di Gennaro, *J. Chem. Soc. Chem. Commun.* **1991**, *22*, 1611; b) L. Santagostini, M. Gullotti, E. Monzani, L. Casella, R. Dillinger, F. Tuczek, *Chem. Eur. J.* **2000**, *6*, 519; c) G. Battaini, M. De Carolis, E. Monzani, F. Tuczek, L. Casella, *Chem. Commun.* **2003**, 726; d) G. Battaini, E. Monzani, A. Perotti, C. Para, L. Casella, L. Santagostini, M. Gullotti, R. Dillinger, C. Näther, F. Tuczek, *J. Am. Chem. Soc.* **2003**, *125*, 4185.

Received: April 25, 2008
Published online: September 11, 2008

